Electronic Supplementary Material (ESI) for Journal of Materials Chemistry C.

SUPPORTING INFORMATION

Detection of nitrophenols with a fluorescent Zr(IV) metal-organic framework functionalized with benzylamino groups

Amina Chatz-Giachia,[a] Athanasia E. Psalti,[a] Anastasia D. Pournara,[b] Manolis J. Manos,[b,c] Christina Pappa,[a] Konstantinos Triantafyllidis,[a] Theodore Lazarides*[a]

[a] Department of Chemistry, Aristotle University of Thessaloniki, 54124, Thessaloniki, Greece
E-mail: tlazarides@chem.auth.gr

[b] Department of Chemistry, University of Ioannina, 45110, Ioannina, Greece

[c] Institute of Materials Science and Computing, University Research Center of Ioannina, 45110, Ioannina, Greece

Table of Contents

Experimental Section

Materials and Methods

All starting materials and solvents were used as received from the usual commercial sources (Sigma Aldrich, Alfa Aesar, Chem-Lab, J&K).

Physical Methods

The NMR spectra of the ligand were recorded at room temperature on an Agilent 500 MHz NMR spectrometer. ^{1}H-NMR spectra were obtained at 500 MHz and ^{13}C-NMR spectra were obtained at 126 MHz with the use of deuterated solvents D_2O and NaOD (1.0 M). The mass spectrum of the ligand was recorded on a (LC-MS) Shimadzu 2010EV instrument. IR spectra were recorded in a scan range from 400 to 4000 cm^{-1} on a Nicolet FT-IR 6700 spectrophotometer equipped with a diamond attenuated total reflection (ATR) stage. Powder X-ray diffraction (PXRD) measurements were performed at room temperature on a on a Bruker D8 Advance X-ray diffractometer with Cu-Ka radiation (k = 1.5418 Å). Thermogravimetric analysis (TGA) was performed on a Perkin Elmer Diamond TG/DTA instrument under air or N_2 atmosphere (200 mL min^{-1}) with a heating rate of 5 ^{o}C min^{-1}. Nitrogen sorption studies were performed at 77 K on a Micromeritics Tristar 3000 instrument and surface areas were calculated according to the BET model. The UV–vis spectra were measured on a Hitachi-2001 spectrophotometer in the wavelength range of 250–500 nm. The fluorescence spectra of solutions and suspensions were measured on an Edinburgh Instruments FS5 spectrofluorometer equipped with a red-sensitive Hamamatsu R13456 photomultiplier tube (PMT) using a 150W Xenon arc lamp. All spectra were corrected for detector response by using the correction files and software (Fluoracle™) provided by the manufacturer. Emission quantum yields were measured using the SC–30 integrating sphere module that consists of a 150 mm inner diameter spherical cavity, constructed from PTFE–based material. Calculation of the quantum yields were carried out using a designated routine within the Fluoracle™ software according to the equation **(S1)** utilizing the emission spectra of the studied sample and a reference sample.

$$\Phi = \frac{Sample\ Emission\ Area - Reference\ Emission\ Area}{Reference\ Scattering - Sample\ scattering} \quad \textbf{(S1)}$$

Synthesis of 2-((benzyl)aminoterephthalic acid (**L-1**)

Ligand **L-1** was prepared according to a two-step procedure previously reported in literature [1] with some modifications. Aminoterephthalic acid (500 mg, 2.80 mmol) and MeOH (40 mL) were added in a 250 mL single mouth round bottom flask and the mixture was stirred in room temperature for 5 min. Benzaldehyde (0.70 mL, 2.5 eq) and triethylamine (1.55 mL, 4 eq) were added and the mixture was refluxed for 5 h under Ar. The reaction yielded a yellow solution containing an intermediate Schiff base. The solution was allowed to cool to room temperature and, afterwards, the flask was placed in ice bath and the solution was stirred at 0 ^{o}C for 10 min. $NaBH_4$ (417 mg, 4.0 eq) was added stepwise and the mixture was stirred at 0 ^{o}C for 2 h and then stirred at room temperature for 20 hr. Evaporation under pressure afforded a yellow solid that was subsequently dissolved in H_2O (14 mL) and MeOH (6 mL). Addition of CH_3COOH (2 mL) to this solution was followed by precipitation of the product **L-1** as yellow solid. The suspension was filtered, and the product was isolated, washed with H_2O and dried in the air. The crude product was recrystallized with a mixture of H_2O and MeOH 1:1 and washed with H_2O to give the final pure product. Yield: 550 mg (2.0 mmol, 73%). ^{1}H-NMR: (D_2O, NaOD, 500 MHz, 298 K): δ (ppm): 7.64 (1 H, d, J = 8 Hz), 7.33 (2 H, d, J = 7 Hz), 7.27 (2 H, dd, J_1 = 15 Hz, J_2 = 7 Hz), 7.19 (1 H, t, J = 15 Hz), 7.13 (1 H, s), 7.00 (1 H, d, J = 8 Hz), 4.35 (2 H, s). ^{13}C-NMR (D_2O/NaOD, 126 MHz, 298 K): δ (ppm): 175.57, 175.53, 148.59, 139.65, 139.42, 131.11, 128.74, 127.38, 127.13, 122.27, 116.57, 113.16, 46.89. IR (KBr pellets, cm^{-1}): 3377 m, 2888 w, 2646 b, 1683 s, 1576 m, 1516 m, 1454 m, 1422 w, 1338 w, 1318 w, 1245 s, 926 w, 874 w, 747 m, 696 w. ESI-MS: (m/z): 272.05 (M-Z).

Synthesis of MOF **Zr-1**

MOF **Zr-1** was synthesized following a slightly modified solvothermal method previously reported in literature. [2] $ZrCl_4$ (162.5 mg, 0.70 mmol) and ligand L-1 (264.5 mg, 1.4 eq) were added in DMF (20 mL) and CH_3COOH (2.50 mL) in a 100 mL Erlenmeyer flask and the mixture was sonicated for *ca.* 3 min. The flask was placed in an oven at 120 ^{o}C for 24 h and then was left to cool to room temperature. The reaction yielded a pale-yellow solid that was washed four times with fresh DMF (6 mL). Afterwards, the product was soaked in DMF (6 mL) for 3 days at room temperature, during which time the solid was isolated via centrifugation and fresh DMF was added three times. The product was then, likewise, soaked in methanol for 3 days with three additions of fresh methanol. This process was carried out to wash out residual reagents trapped inside the structure's pores. After removal of methanol by centrifugation, the sample was dried at 50 °C for 24 h to yield the final product. Yield: 270 mg. IR (KBr pellets, cm^{-1}): 3382 b, 2981 w, 1656 w, 1622 w, 1574 s, 1497 w, 1440 m, 1386 s, 1311 w, 1281 w, 1256 w, 765 m, 667 m, 477 m. The stability of ligand **L-1** after incorporation into the

MOF's structure was established by ^{1}H-NMR study of digested material. In a typical procedure, 8 mg of Zr-1 was dissolved in 40% NaOD in D_2O, the mixture was sonicated for 5 min and then centrifugated for 10 min. The supernatant was directly transferred to an NMR tube for analysis. The spectrum obtained for Zr-1 is identical to the ^{1}H-NMR spectrum for the ligand **L-1** apart from some weak additional peaks corresponding to <10% aminoterephthalic acid due to partial elimination of benzyl groups during MOF synthesis. (The three peaks corresponding to aminoterephthalic acid are found at δ (ppm) 7.56, 7.13, 7.06 ppm.

Activation of MOF **Zr-1** (**pZr-1**)

Zr-1 (100 mg) was added to H_2O (10 mL), stirred for 30 min and isolated via centrifugation. The H_2O treatment was repeated once more. Afterwards, the sample was mixed with 4.0 M HCl solution (20 mL), stirred for 8 hr and consequently isolated via centrifugation affording a protonated material. The activated sample was soaked in methanol (6 mL) for 3 days at room temperature, during which time the solid was isolated via centrifugation and fresh methanol was added three times. The product was isolated via centrifugation, dried at 50 °C for 24 h and was used in fluorescence measurements and sorption studies.

The stability of ligand **L-1** into the activated MOF's structure was examined by ^{1}H-NMR study after MOF digestion in 40% NaOD in D_2O. It is demonstrated by the ^{1}H-NMR spectra that treatment with 4.0 M HCl solution results in benzyl group elimination to a rate of approximately 30%.

Titration studies

In a typical procedure **pZr-1** (1 mg) was dispersed in 10 ml of H_2O at pH 4.5. The system was sonicated for *ca.* 10 min. and 2 mL were transferred to a quartz cuvette. The fluorescence spectrum of the suspension was recorded multiple times in the span of 30 minutes to ensure its stability and calculate the standard deviation of the measurement. (λ_{exc} = 400 nm) Aliquots of the analyte aqueous solution were added to the suspension using a precision Hamilton microsyringe (50 μL range). Fluorescence spectra were recorded following each analyte addition after *ca*. 30 s of magnetic stirring.

Quantum yield measurements

The emission quantum yields of **Zr-1**, **pZr-1** and UiO-66-NH_2 were measured on MOF suspensions in H_2O, as prepared for titration studies (0.1 mg mL^{-1}). The emission quantum yields of **L-1** and NH_2bdc were measured on solutions in MeOH. The solutions absorbance at the λ_{exc} was adjusted to 0.1.

Kinetic study

2 mL of **pZr-1** dispersed in H_2O (as prepared for titration studies) were transferred to a quartz cuvette. Time-depended emission intensity was recorded (λ_{exc} = 400 nm, λ_{em} = 470 nm) while 10 µL of TNP (10^{-3} M) were added to the suspension. The suspension was under magnetic stirring throughout the experiment.

Characterization of L-1

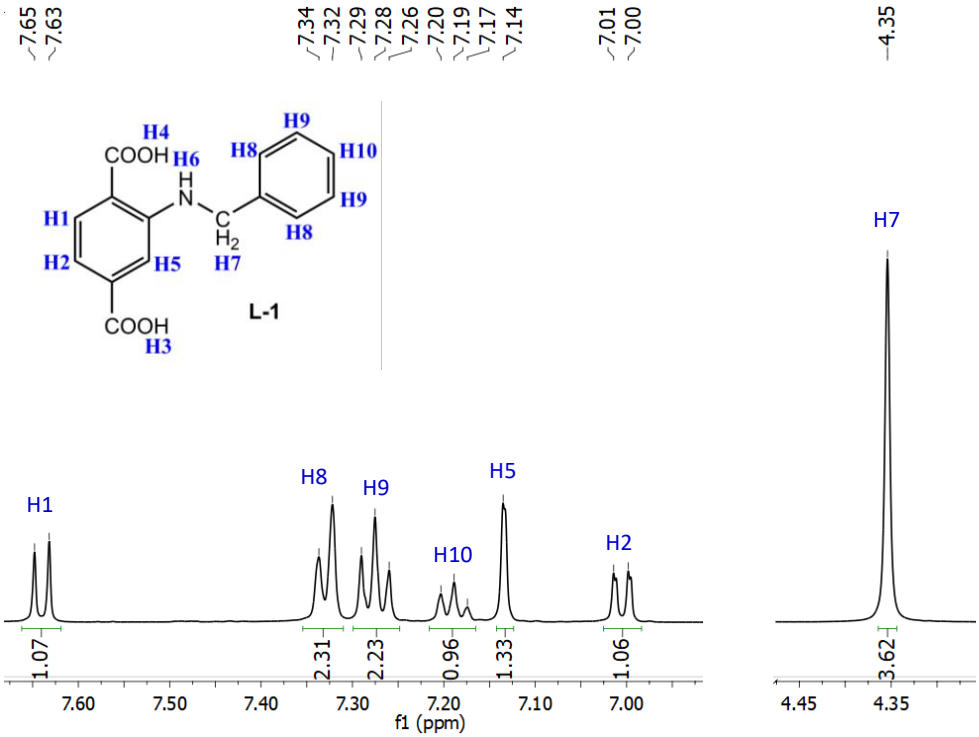

Figure S1. ^{1}H-NMR spectrum of ligand **L-1** in D_2O/NaOD.

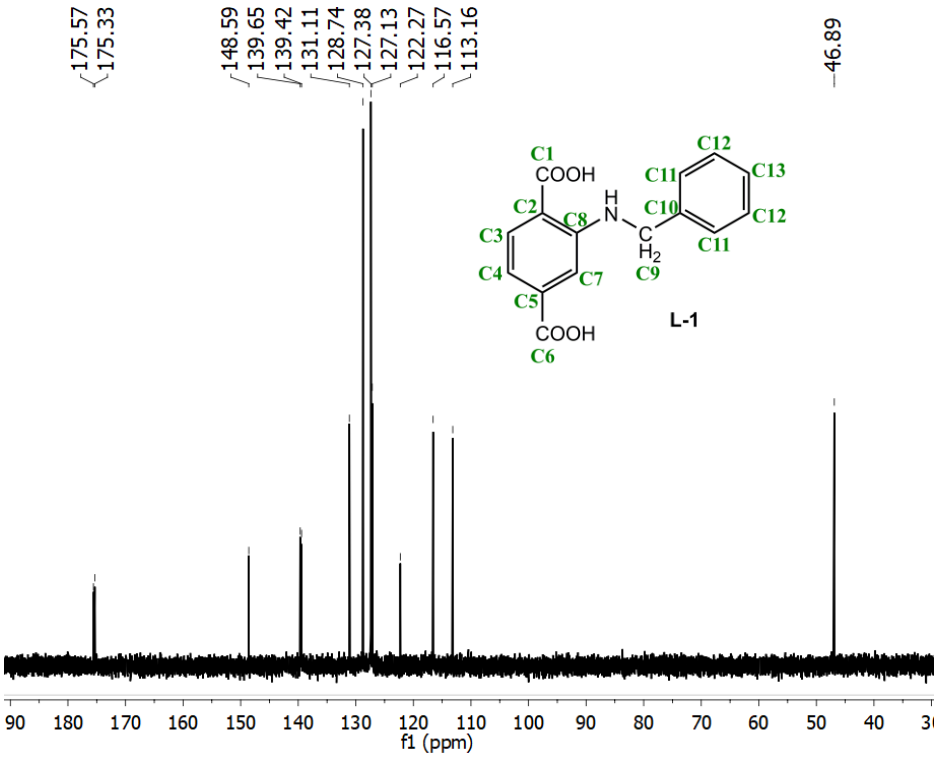

Figure S2. ^{13}C NMR spectrum of ligand **L-1** in D_2O/NaOD. We observe 13 peaks, as expected according to the numbered scheme.

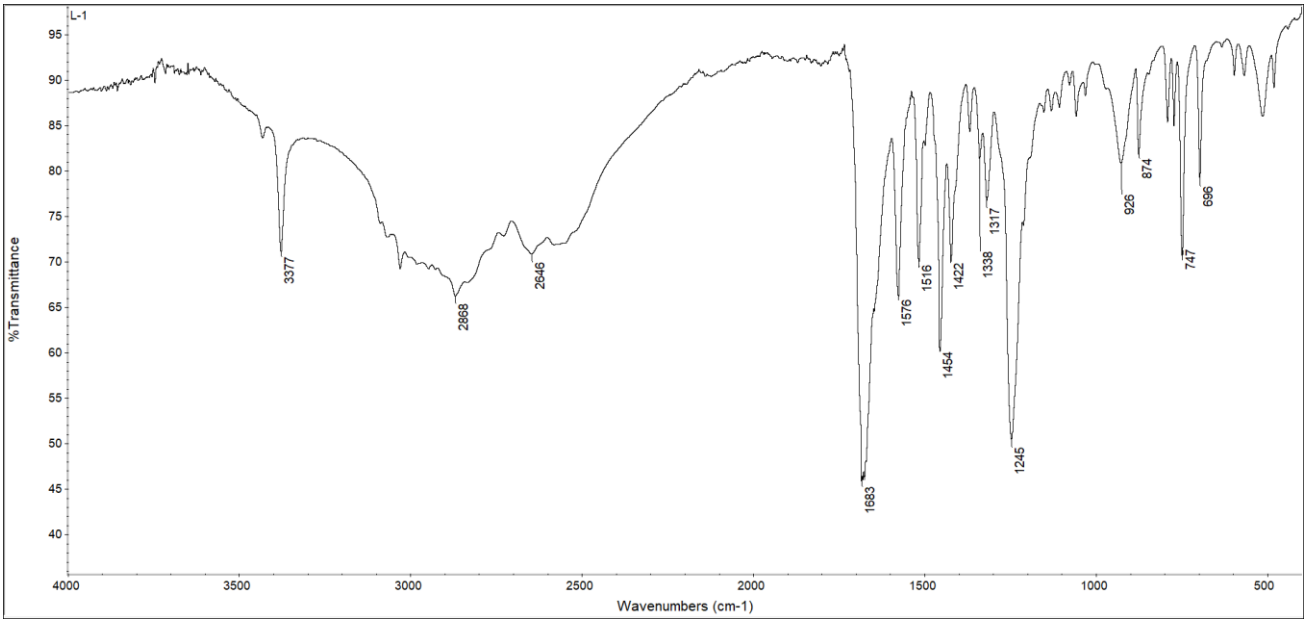

Figure S3. IR spectrum of ligand **L-1**.

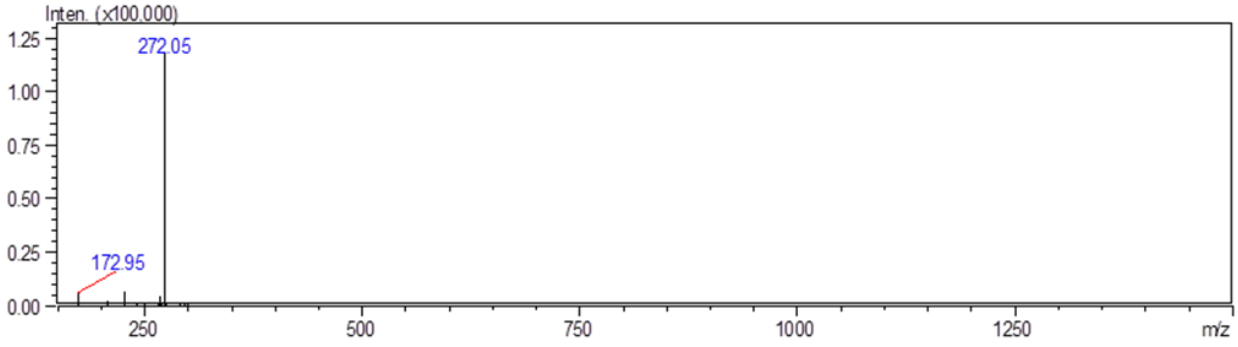

Figure S4. Mass spectrum (ESI-MS) of ligand **L-1**.

Characterization of Zr-1 and pZr-1

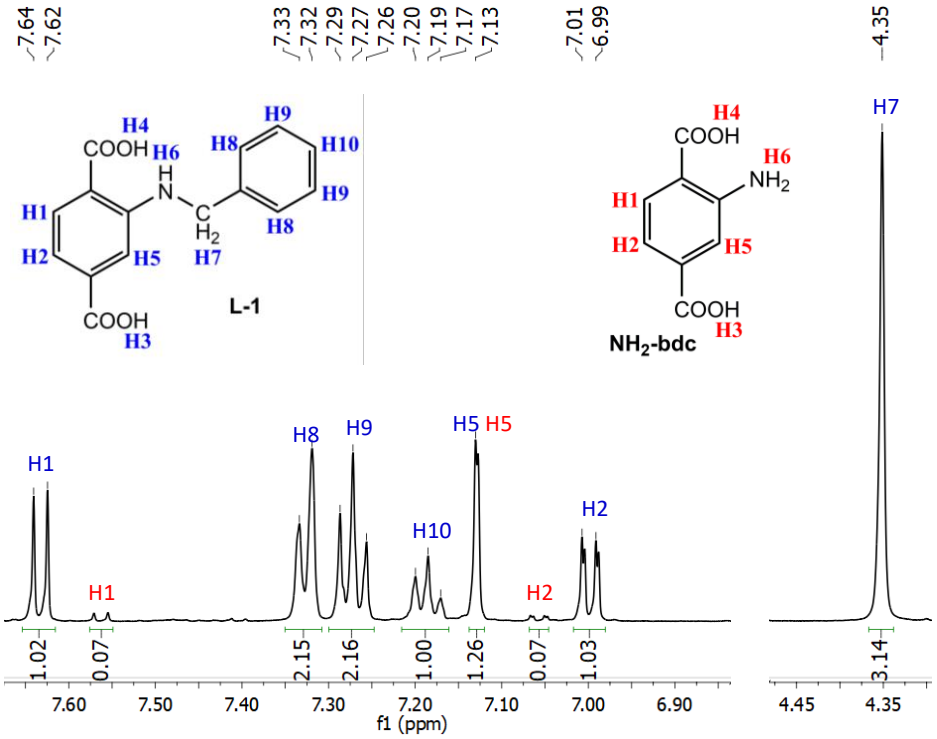

Figure S5. ^{1}H-NMR spectrum of **Zr-1** digested in D_2O/NaOD.

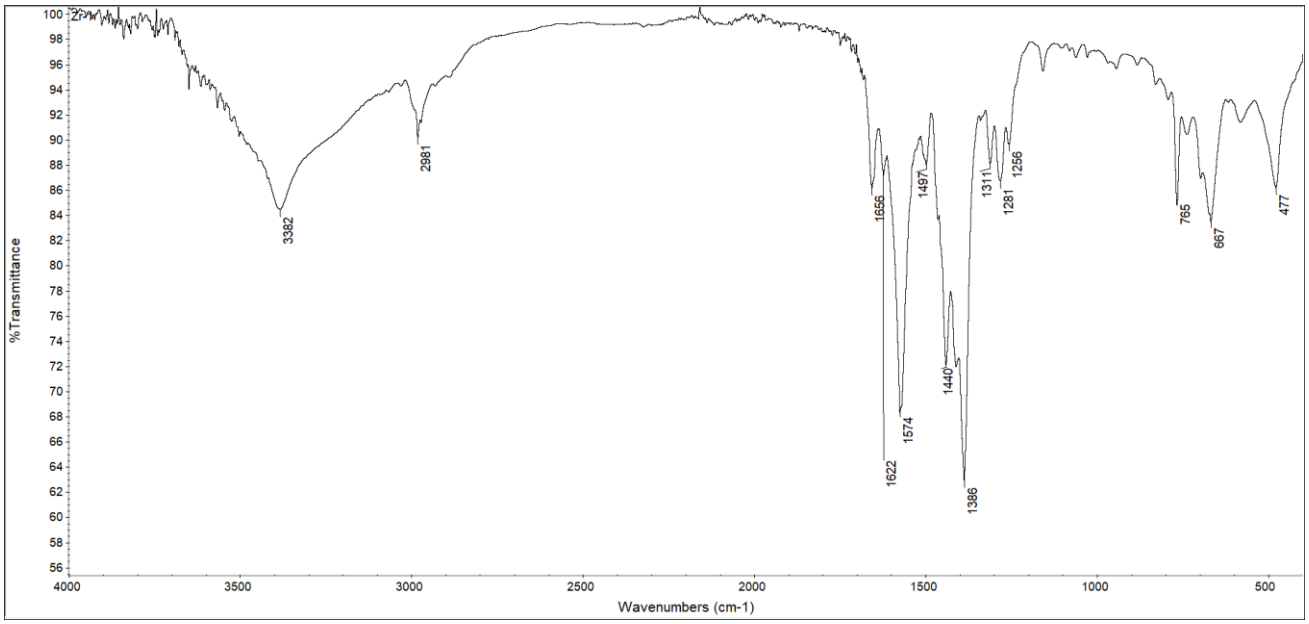

Figure S6. IR spectrum of **Zr-1**.

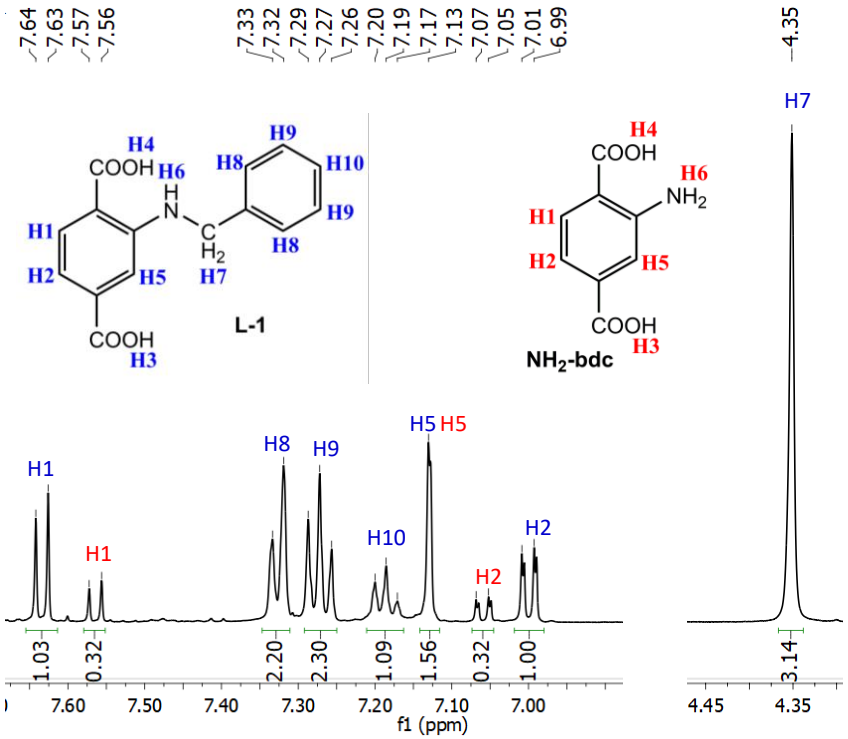

Figure S7. ^{1}H-NMR spectrum of **pZr-1** digested in D_2O/NaOD.

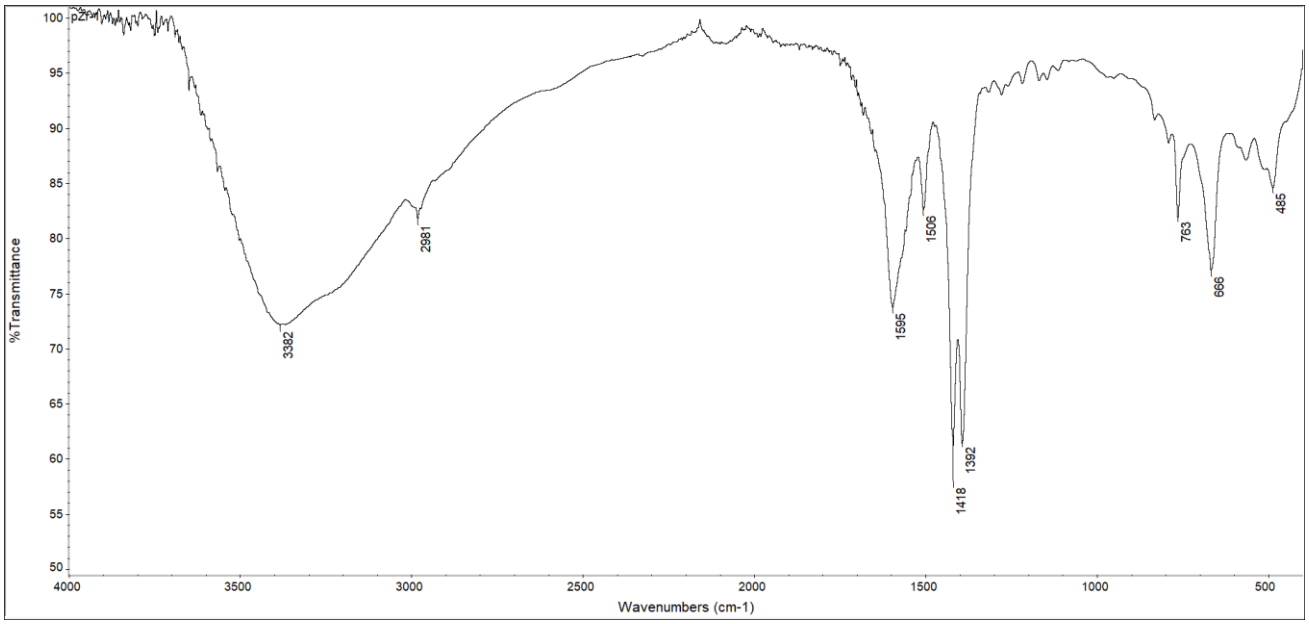

Figure S8. IR spectrum of **pZr-1**

Thermal stability

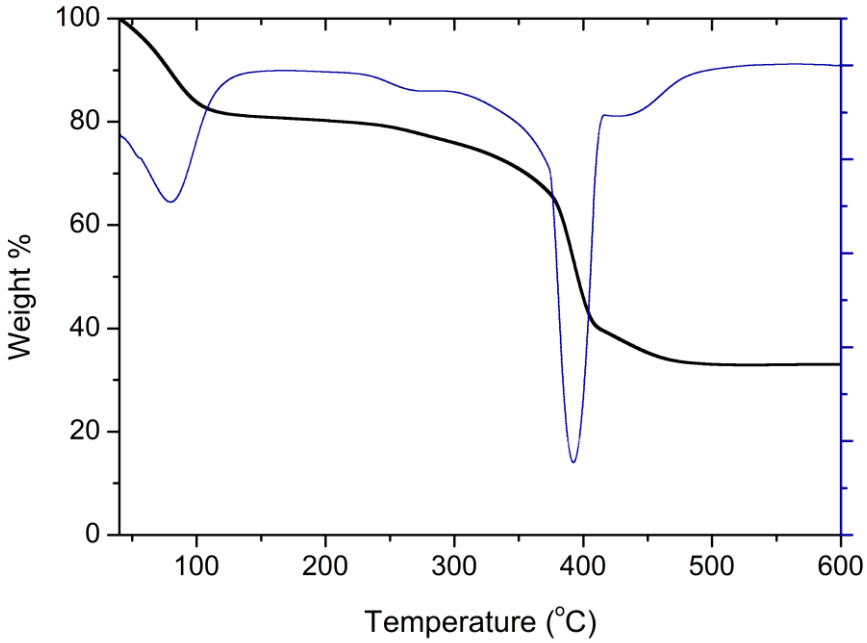

Figure S9. TGA curve of **Zr-1** after H_2O exchange under air (black line) and first derivative (blue line).

The thermogravimetric data for **Zr-1** reveal that weight loss occurs in two main steps: the first, completed at *ca.* 175 ℃, corresponds to removal of lattice solvents that leads to the sample's weight reduced to 80.59% and the second, completed at ca. 550 ℃, corresponds to release of organic linkers and formation of ZrO_2[3] with the final weight reduced to 32.90%. (Each step's completion temperature is determined according to the corresponding plateau of the first derivative of the TGA curve.) The experimental Zr content by weight of ZrO_2 residue is calculated to be 30.22%. The expected Zr content by weight would be 24.37% for a 12-connected material with the formula $\{Zr_6O_4(OH)_8(H_2O)_4$(**L-1**$)_{5.4}(NH_2bdc)_{0.6}\}$ and 29.36% for an 8-connected material with the formula $\{Zr_6O_4(OH)_8(H_2O)_4$(**L-1**$)_{3.6}(NH_2bdc)_{0.4}\}$. Our experimentally determined Zr content by weight value of 30.22% agrees with **Zr-1** having an average connectivity of 8.

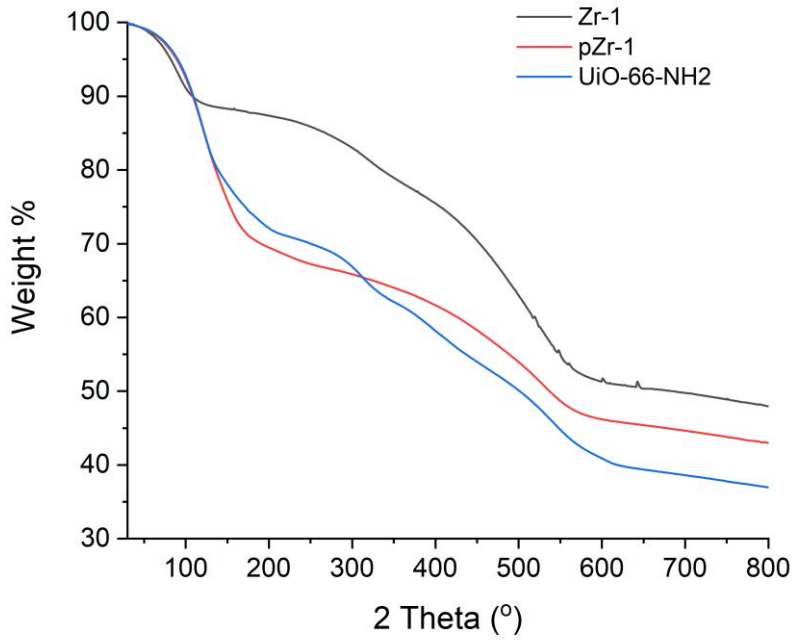

Figure S10. TGA curves of H_2O treated **Zr-1** (gray line), **pZr-1** (red line) and UiO-66-NH2 (blue line) under N_2 flow.

BET surface area

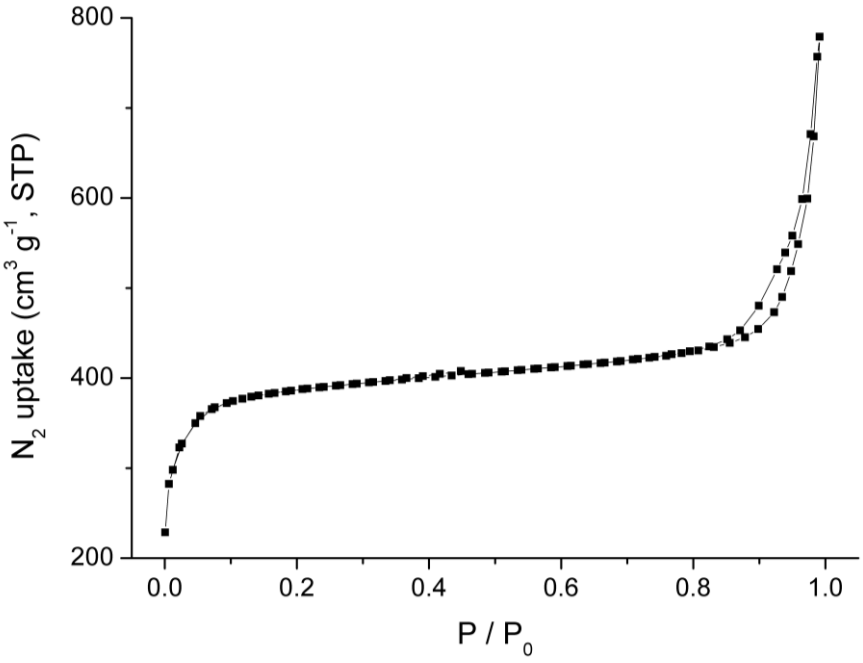

Figure S11. Nitrogen sorption isotherm at 77 K of UiO-66-NH_2 after treatment with acetone and overnight evacuation (120℃). BET surface area: 1274 m^2 g^{-1}.

Photophysical Properties

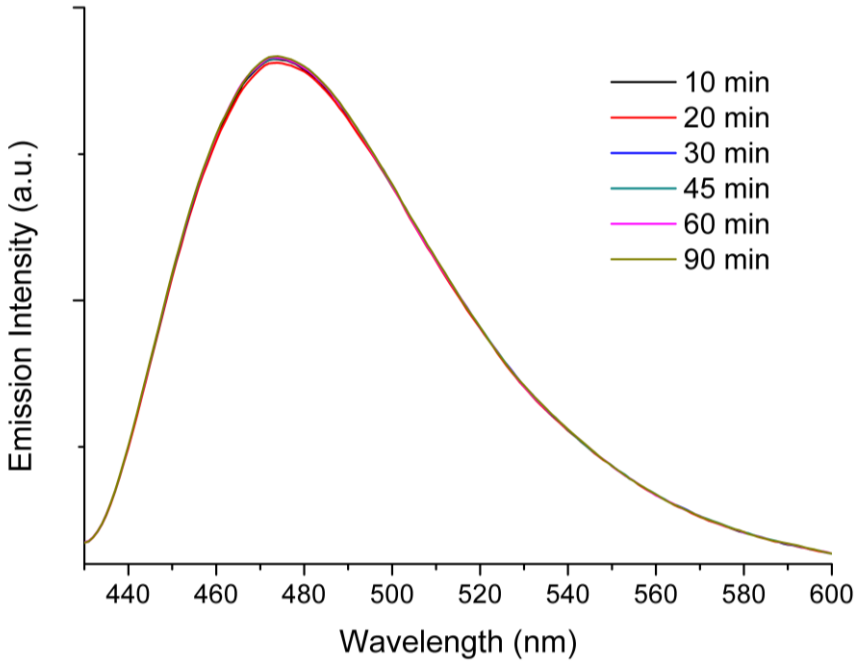

Figure S12. Emission intensity of **pZr-1** suspended in H_2O (2 mL, 0.1 mg mL^{-1}) at pH 4.5 measured in the span of 90 minutes (λ_{exc} = 400 nm)

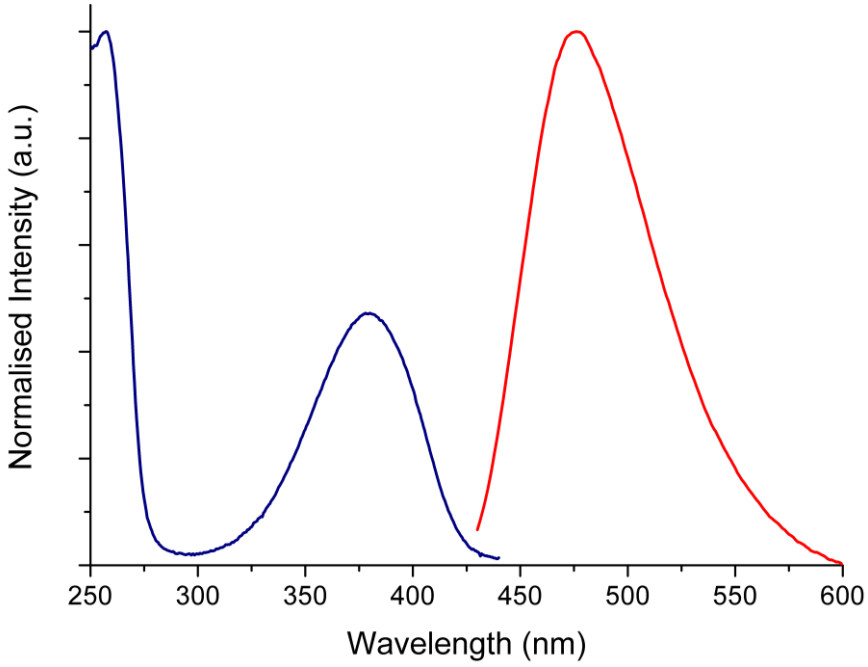

Figure S13. Normalized UV-Vis absorption spectrum (blue line) and emission spectrum (red line) of ligand **L-1** in MeOH solution.

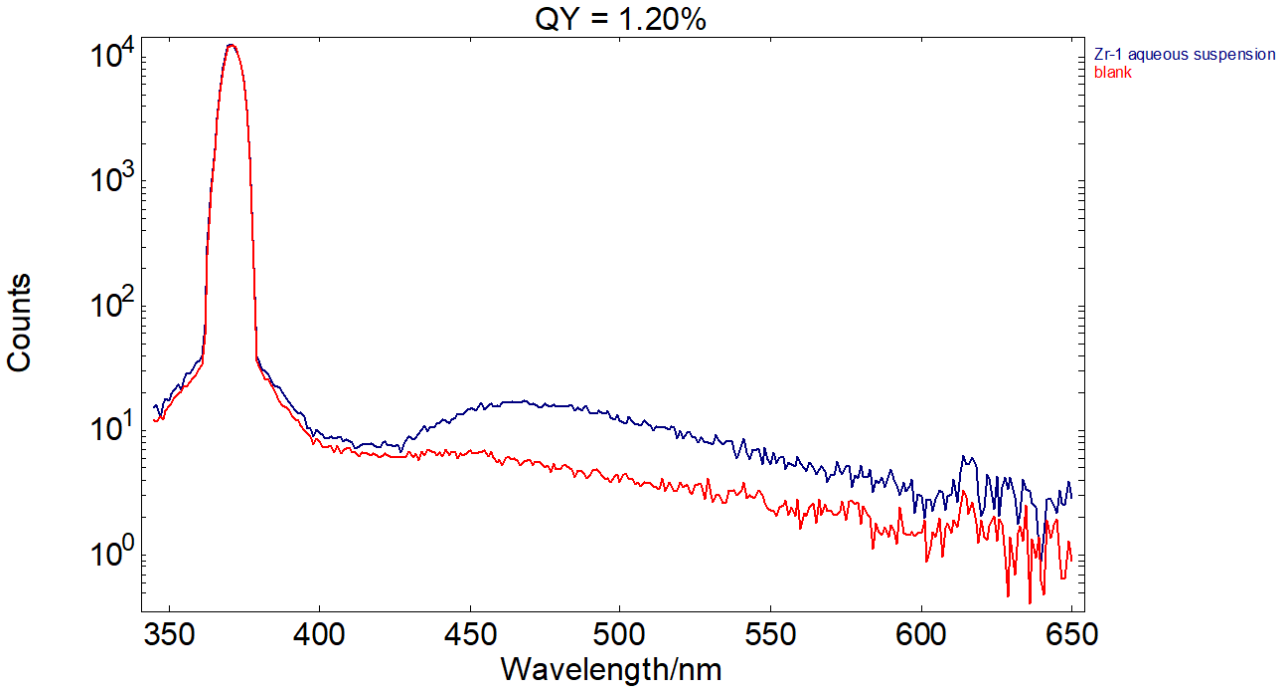

Figure S14. Emission quantum yield of **Zr-1** suspended in H_2O (0.1 mg mL^{-1}).

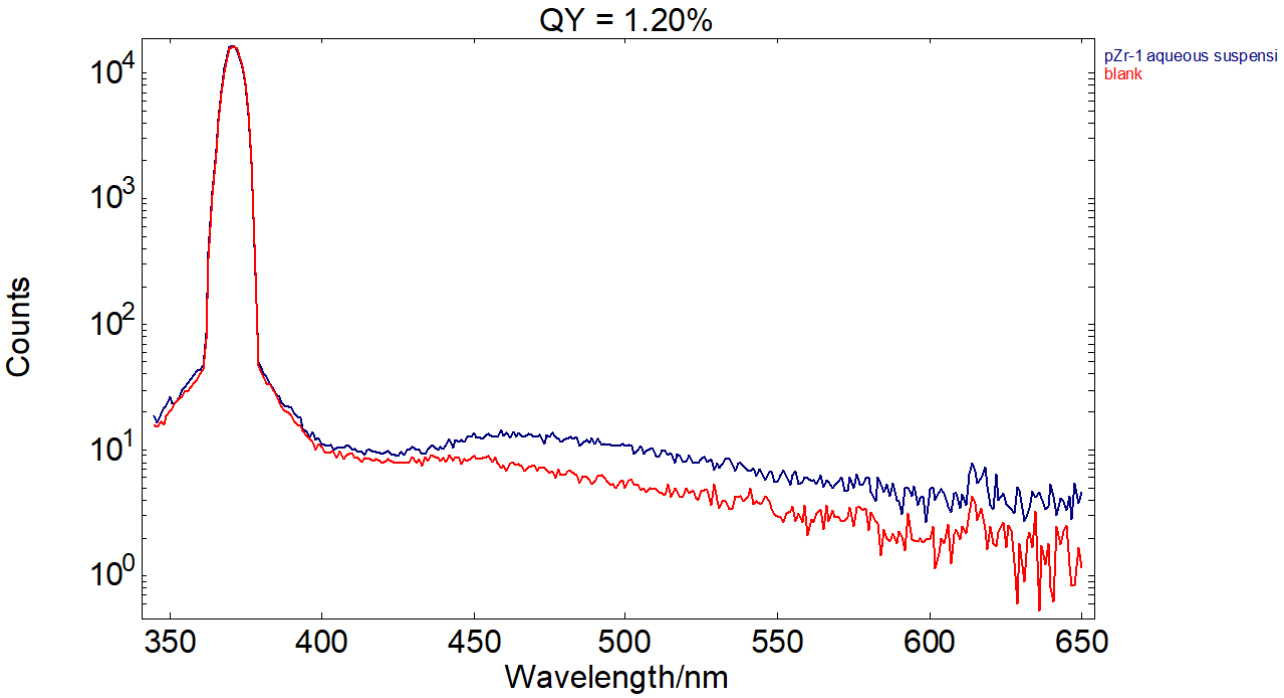

Figure S15. Emission quantum yield of **pZr-1** suspended in H_2O (0.1 mg mL^{-1}).

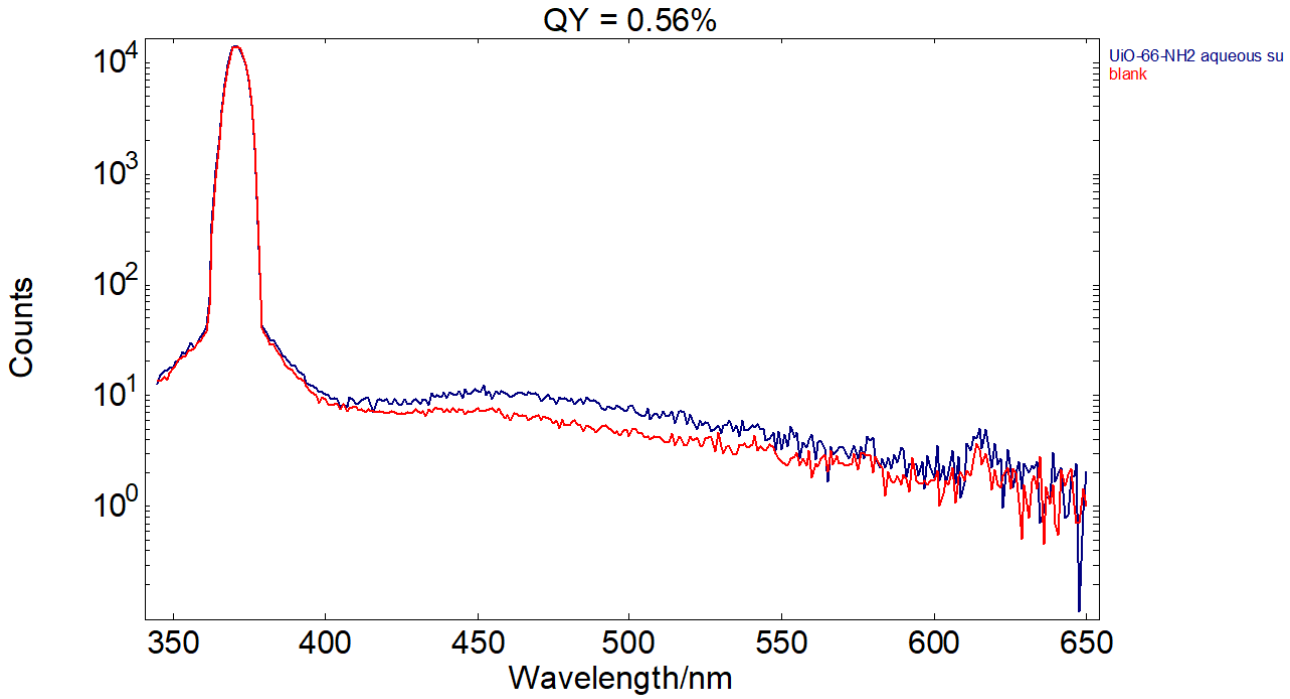

Figure S16. Emission quantum yield of UiO-66-NH_2 suspended in H_2O (0.1 mg mL^{-1}).

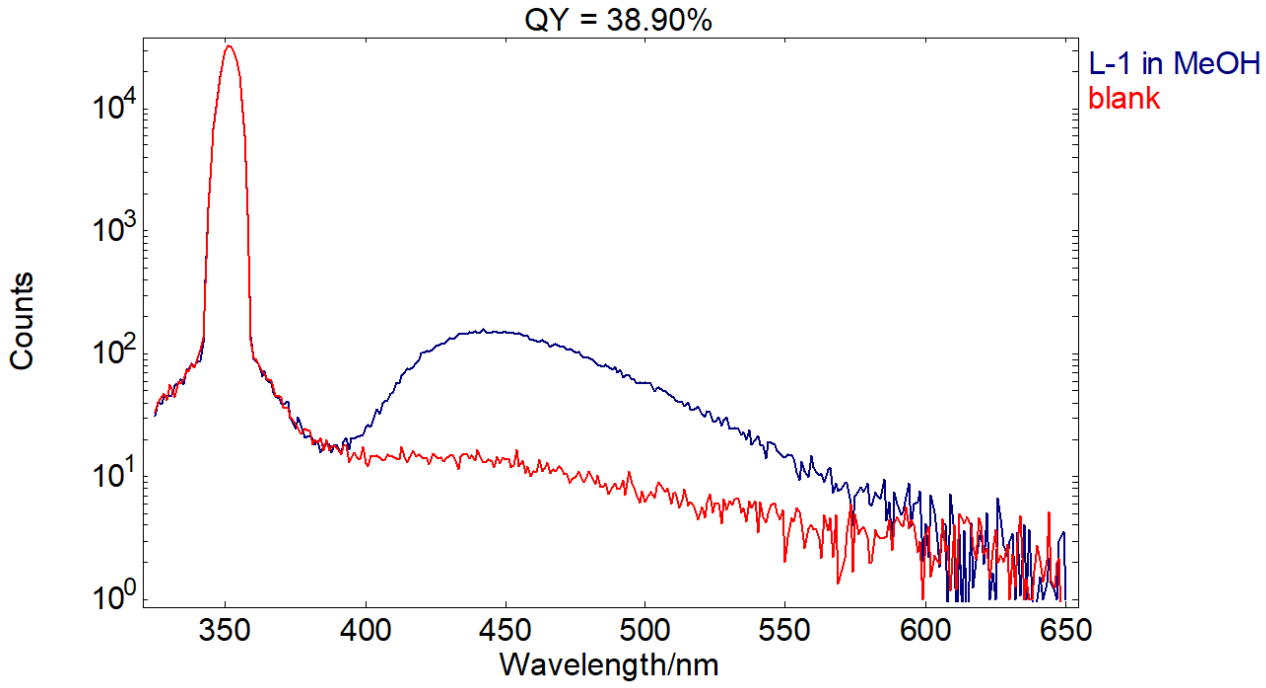

Figure S17. Emission quantum yield of **L-1** in MeOH solution. The solution absorbance at the λ_{exc} was adjusted to 0.1.

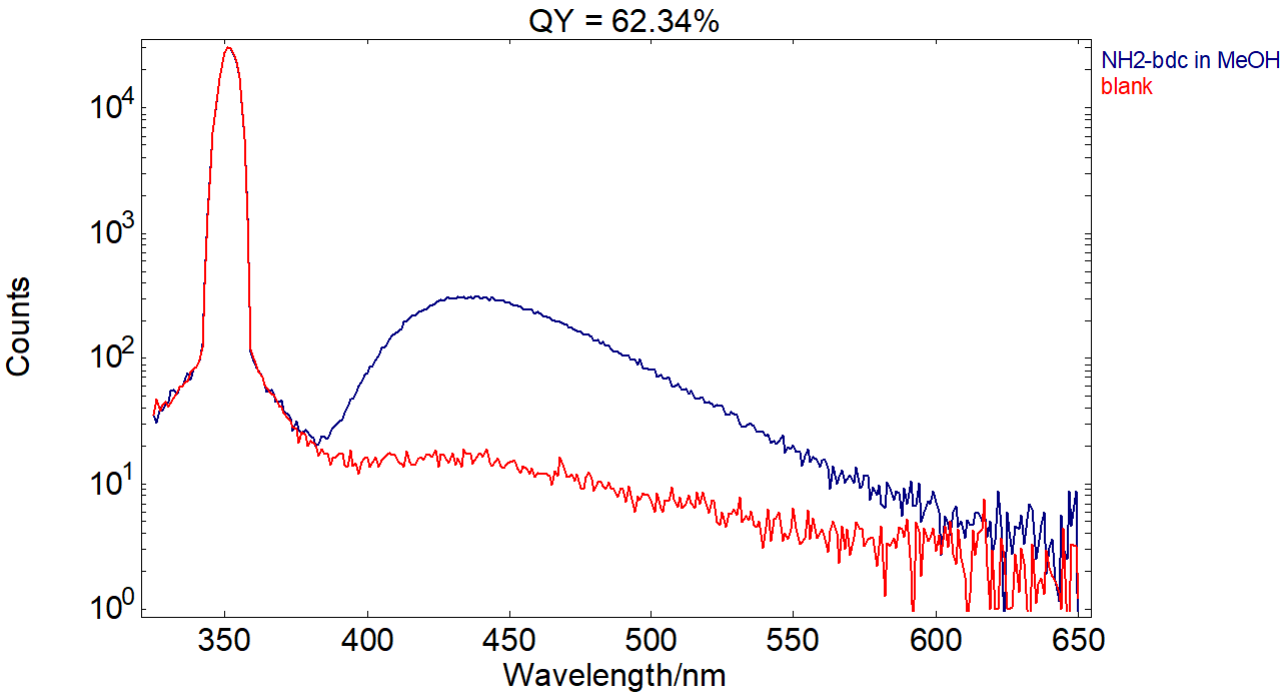

Figure S18. Emission quantum yield of NH_2bdc in MeOH solution. The solution absorbance at the λ_{exc} was adjusted to 0.1.

Fluorescence Titrations

Inner Filter Effect (IFE)

The absorption spectra of DNP and TNP in aqueous solutions (5.0×10^{-5} M) can be seen in Figure S19. Both analytes exhibit strong absorptions in the near-UV region with maxima at *ca.* 360 and 350 nm respectively, with their absorption bands tailing off at *ca.* 470 nm.

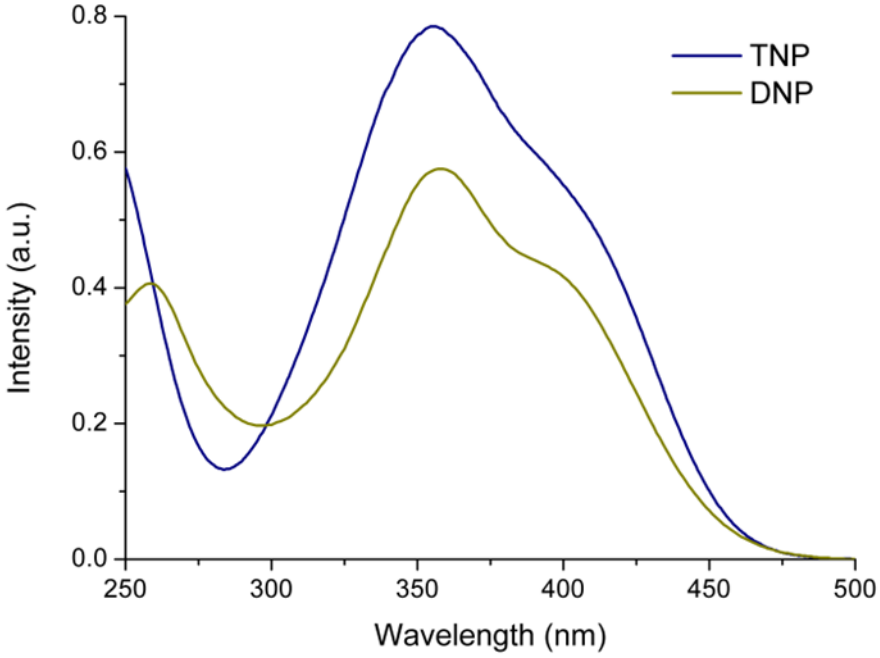

Figure S19. UV-Vis absorption spectra of aqueous solutions of TNP and DNP (5×10^{-5} M)

The UV-Vis absorption spectra of analytes DNP and TNP overlap to a small extent with the excitation wavelength used in the fluorescence titrations of **pZr-1** (400 nm). This may result to a slight decrease in the measured fluorescence intensity known as Inner Filter Effect (IFE). To ensure the accuracy of our results, we applied IFE correction to all our experimental data.

The corrected fluorescence intensity is given approximately by the following equation:

$$I_{corr} = I_{obs} \times 10^{(A_{exc}+A_{em})/2} \quad \textbf{(S2)}$$

where I_{corr} is the corrected fluorescence intensity; I_{obs} is the measured fluorescence intensity; A_{exc} and A_{em} represent the absorbance at the excitation wavelength (λ_{exc}) and the emission (λ_{em}) wavelength, respectively.[4]

The IFE corrected titration data were used in the calibration curves and Stern-Volmer plots. It is important to note that, at the low analyte concentrations of our experiments, IFE correction does not result in significant alteration of the initial titration data. This is demonstrated by a comparative

plot (Figure S20) of calibration curves with corrected and uncorrected data for the fluorescence titration with TNP shown in Figure 5a.

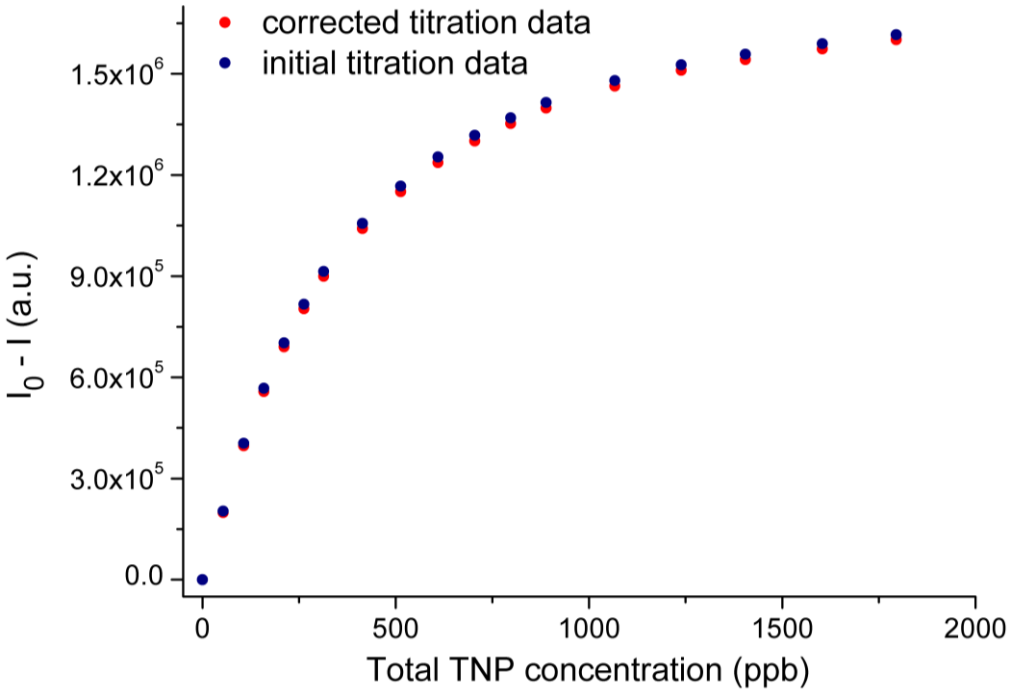

Figure S20. Comparison of the calibration curves consisting of IFE corrected and uncorrected data for the fluorescence titration (λ_{exc} = 400 nm) of **pZr-1** suspended in H_2O (2 mL, 0.1 mg mL^{-1}) at pH 4.5 upon gradual addition of aqueous solution of TNP (5×10^{-5} M).

Limit of Detection (LOD) and Limit of Quantitation (LOQ)

The LOD and LOQ values are calculated using the following equations[5]:

$$LOD = \frac{3 \times SD}{\sigma} \quad \textbf{(S3)}$$

$$LOQ = \frac{10 \times SD}{\sigma} \quad \textbf{(S4)}$$

where *SD* is the standard deviation of the measurement of the initial fluorescence intensity, I_0, and σ is the slope of the linear fitting on the initial part of the calibration curve.

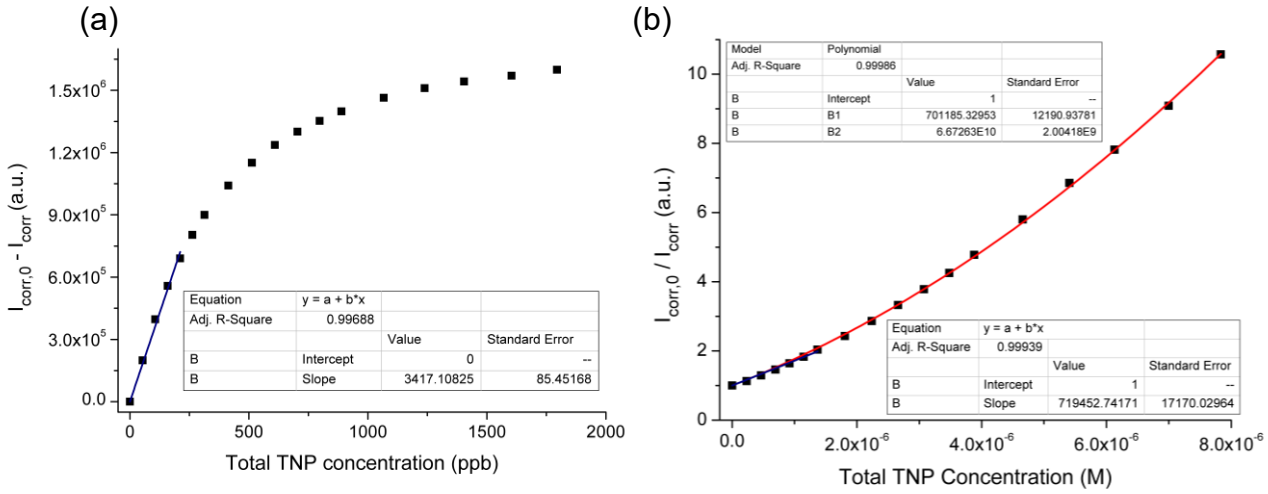

Figure S21. (a) Calibration curve and (b) Stern-Volmer plot of the fluorescence titration (λ_{exc} = 400 nm) of **pZr-1** suspended in H_2O (2 mL, 0.1 mg mL^{-1}) at pH 4.5 upon gradual addition of aqueous solution of TNP (5×10^{-5} M).

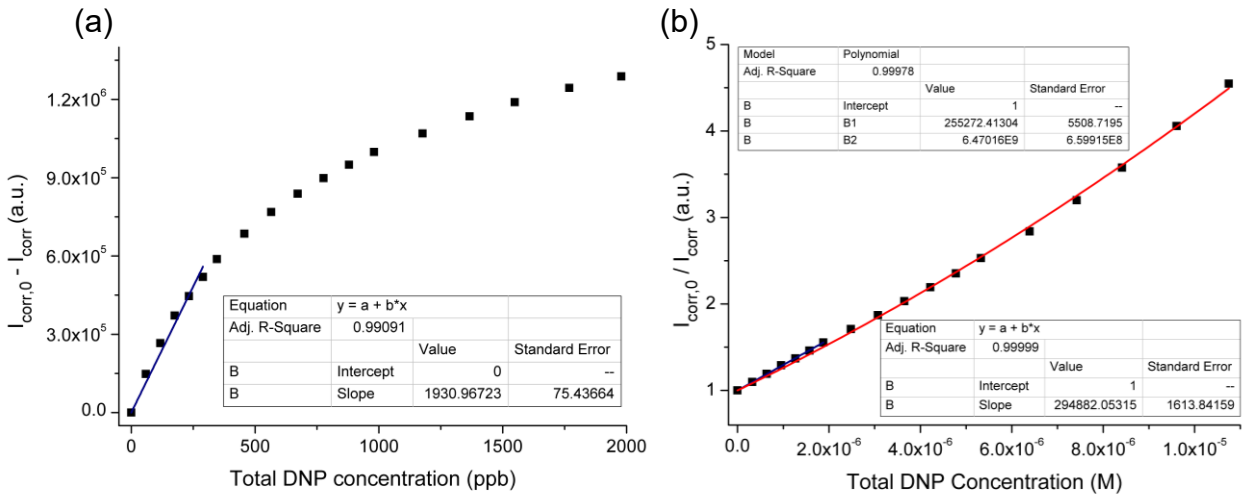

Figure S22. (a) Calibration curve and (b) Stern-Volmer plot of the fluorescence titration (λ_{exc} = 400 nm) of **pZr-1** suspended in H_2O (2 mL, 0.1 mg mL^{-1}) at pH 4.5 upon gradual addition of aqueous solution of DNP (5×10^{-5} M).

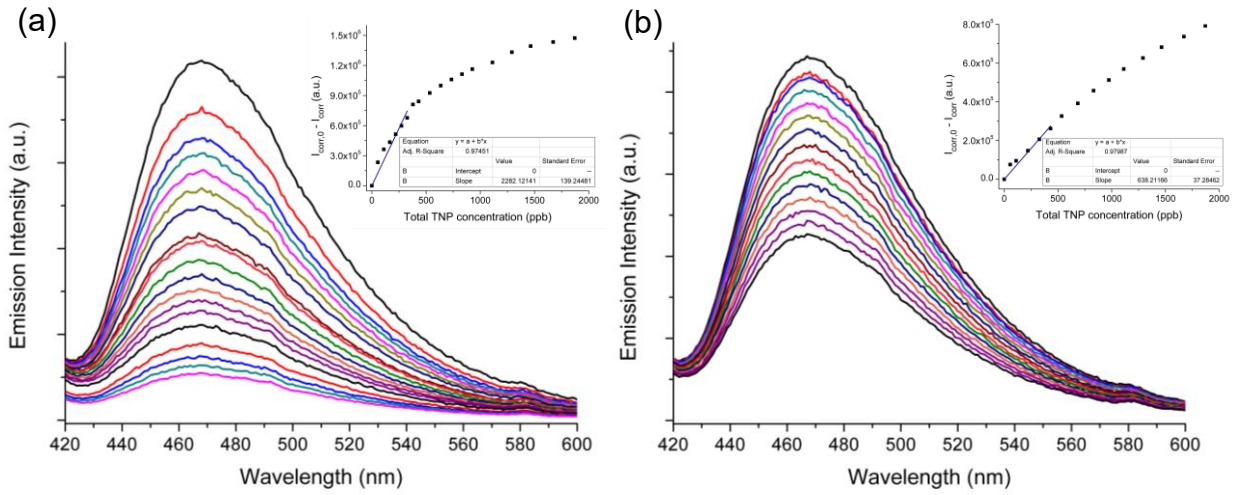

Figure S23. Fluorecence titrations (λ_{exc} = 400 nm) of (a) **Zr-1** and (b) deprotonated **Zr-1** (treated with TEA/MeOH solution), suspended in H_2O (2 mL, 0.1 mg mL^{-1}) at pH 4.5 upon gradual addition of aqueous solution of TNP (5×10^{-5} M). (Inset: Corresponding calibration curves)

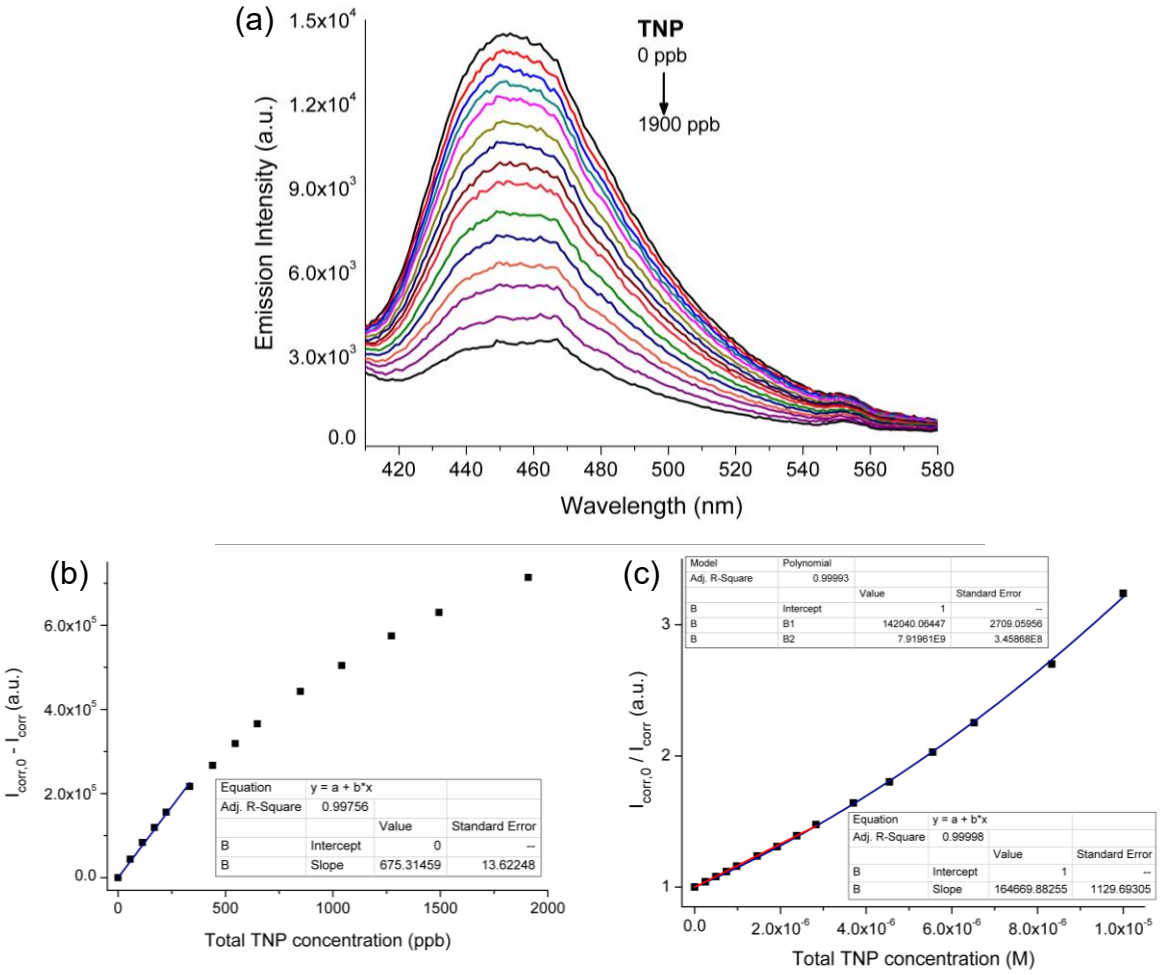

Figure S24. (a) Fluorecence titration (λ_{exc} = 400 nm) of acid activated UiO-66-NH_2 suspended in H_2O (0.1 mg mL^{-1}) at pH 4.5 upon gradual addition of aqueous solution of TNP (5×10^{-5} M) with the corresponding (b) calibration curve and (c) Stern-Volmer plot.

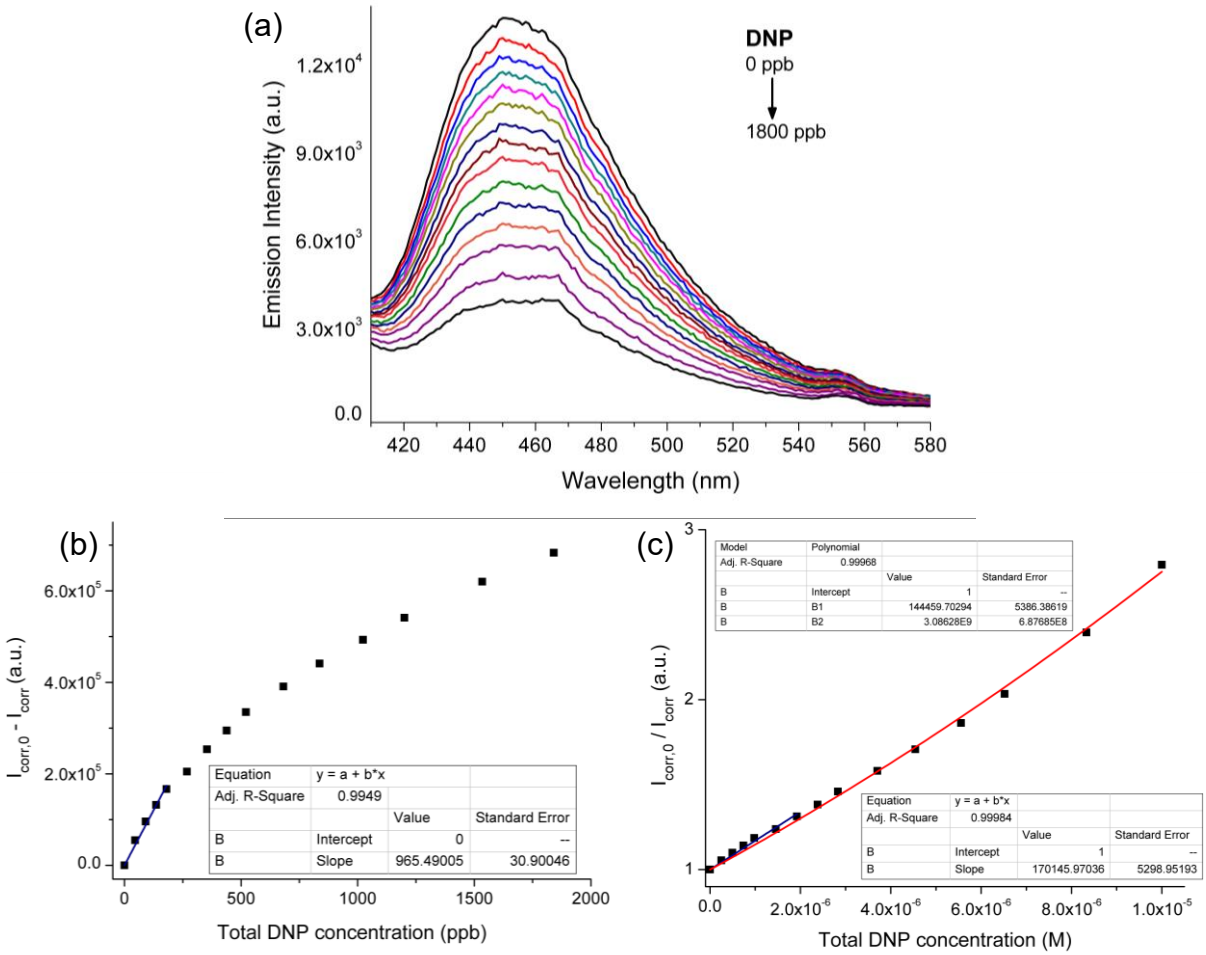

Figure S25. (a) Fluorecence titration (λ_{exc} = 400 nm) of acid activated UiO-66-NH_2 suspended in H_2O (2 mL, 0.1 mg mL^{-1}) at pH 4.5 upon gradual addition of aqueous solution of DNP (5 × 10^{-5} M) with the corresponding (b) calibration curve and (c) Stern-Volmer plot.

Selectivity study

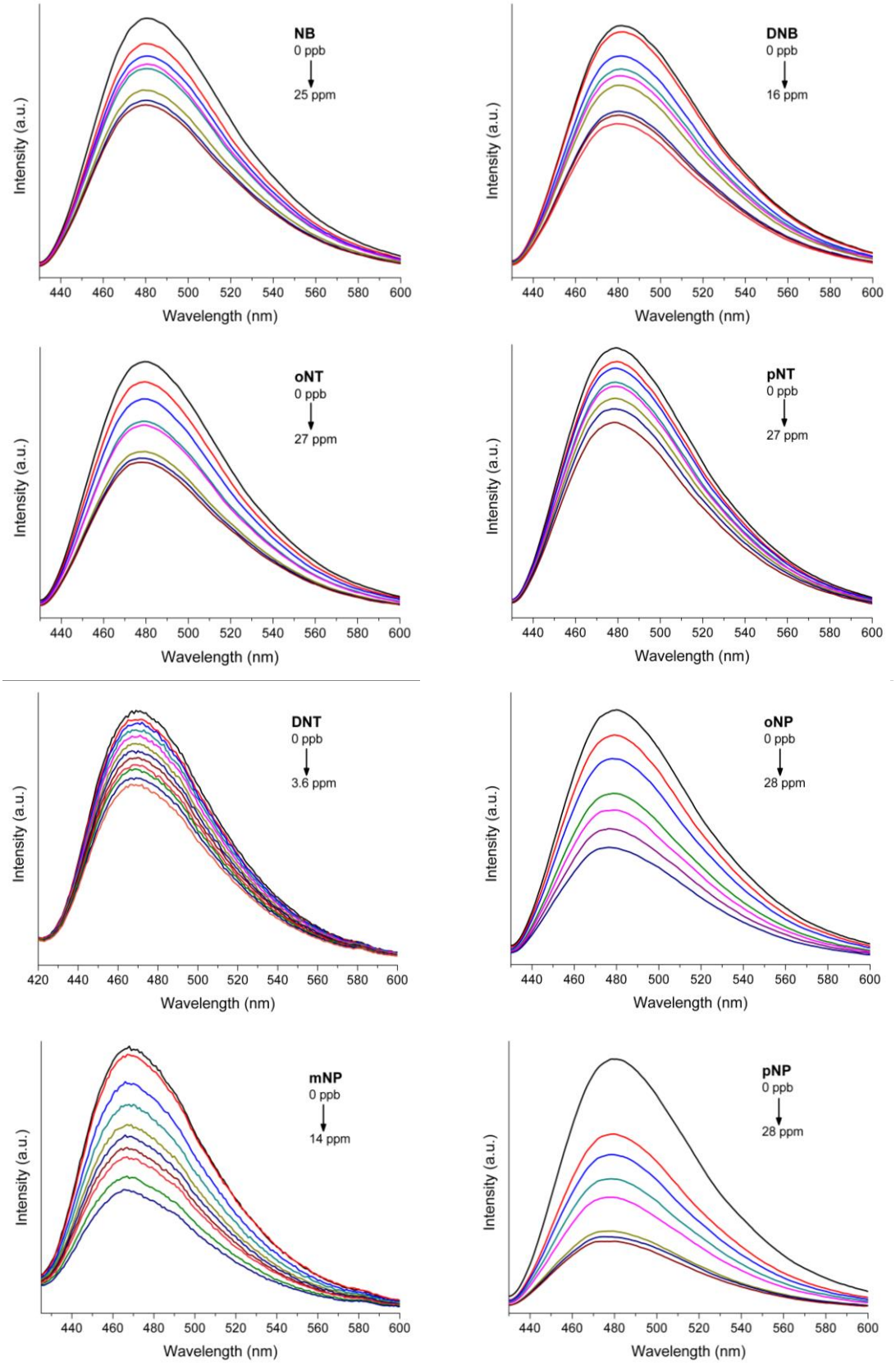

Figure S26. Fluorescence titrations (λ_{exc} = 400 nm) of **pZr-1** suspended in H_2O (2 mL, 0.1 mg mL^{-1}) at pH 4.5 upon gradual addition of aqueous solution of different nitroaromatic analytes.

Sorption, kinetic, recyclability study

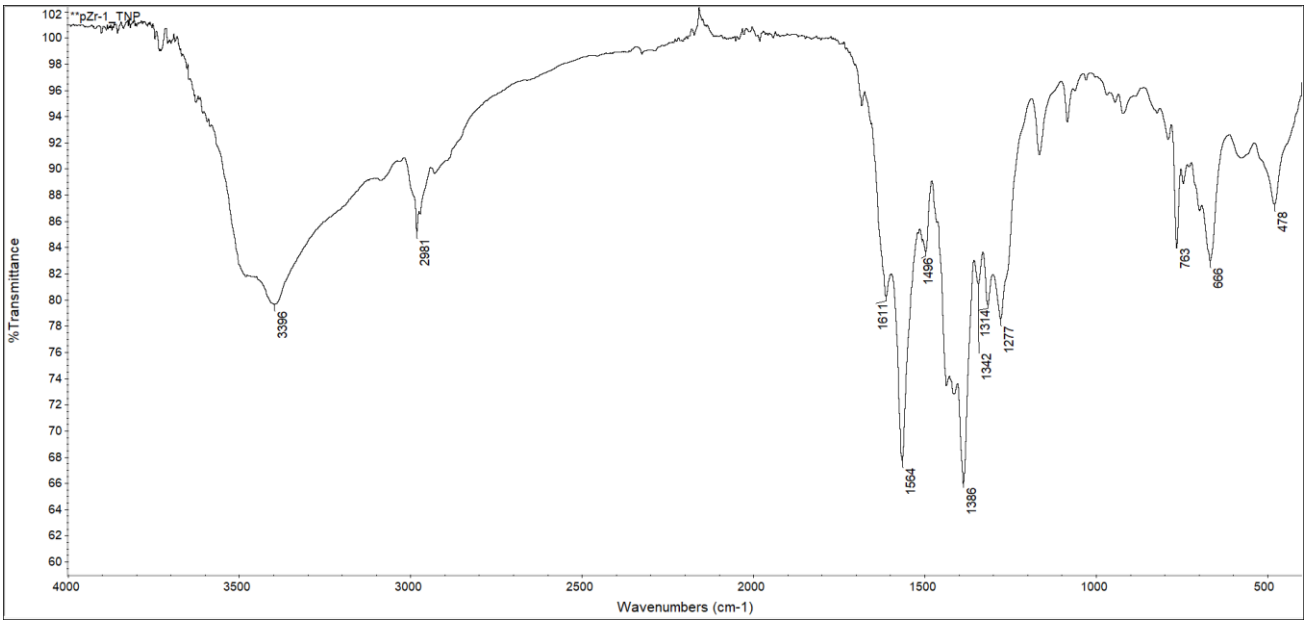

Figure S27. IR spectrum of **pZr-1** after TNP sorption and overnight MeOH treatment.

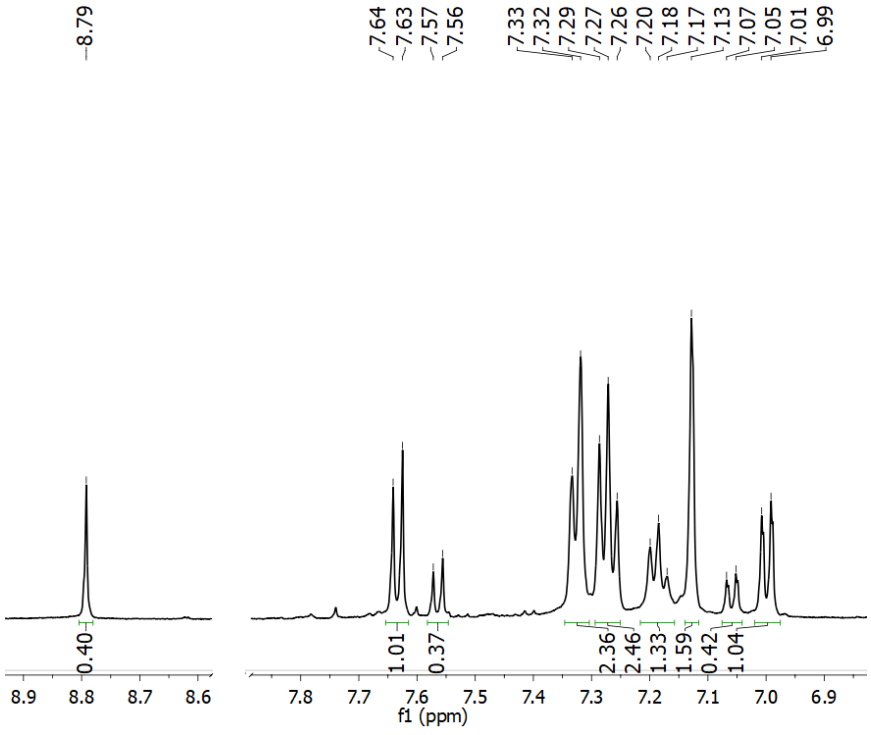

Figure S28. ^{1}H-NMR spectrum (aromatic region) of **pZr-1** after TNP sorption and overnight MeOH treatment, digested in D_2O/NaOD. Peak corresponding to TNP found at δ (ppm) 8.79.

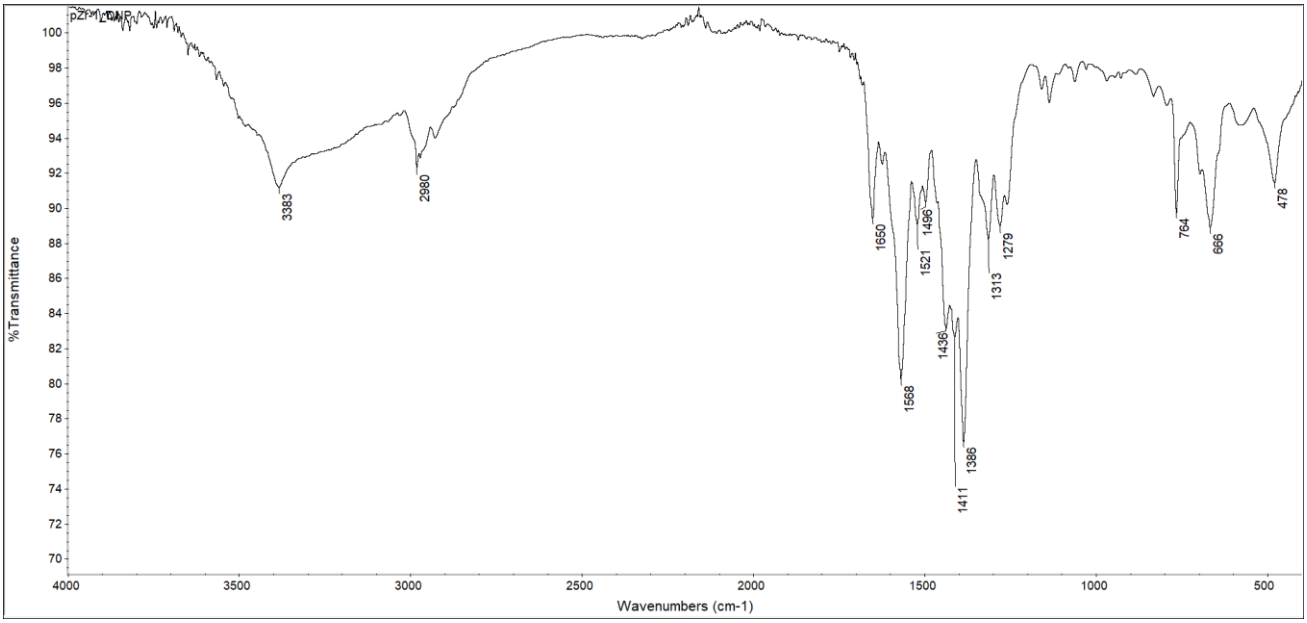

Figure S29. IR spectrum of **pZr-1** after DNP sorption and overnight MeOH treatment.

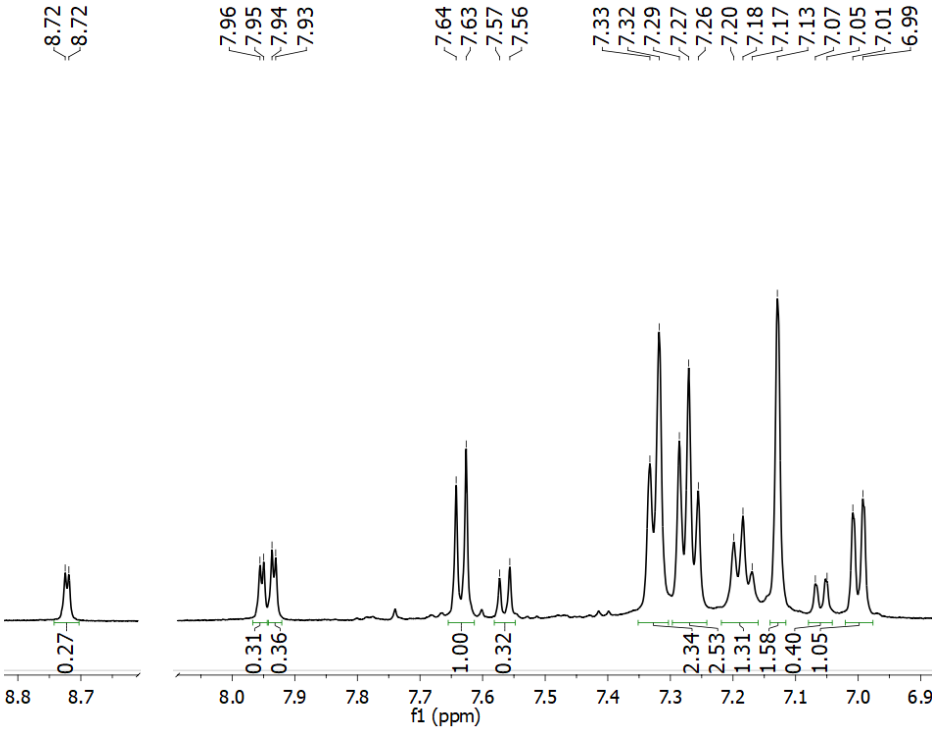

Figure S30. ^{1}H-NMR spectrum (aromatic region) of **pZr-1** after DNP sorption and overnight MeOH treatment, digested in D_2O/NaOD. Peaks corresponding to DNP found at δ (ppm) 8.72, 7.96, 7.94.

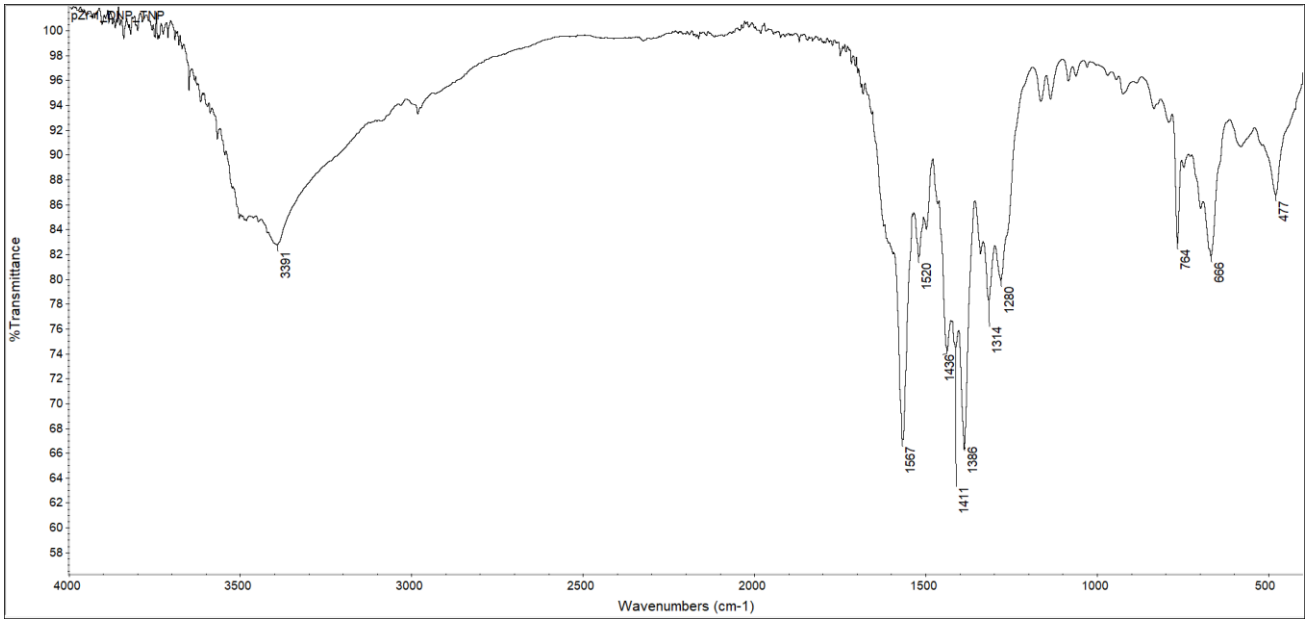

Figure S31. IR spectrum of **pZr-1** after DNP/TNP sorption and overnight MeOH treatment.

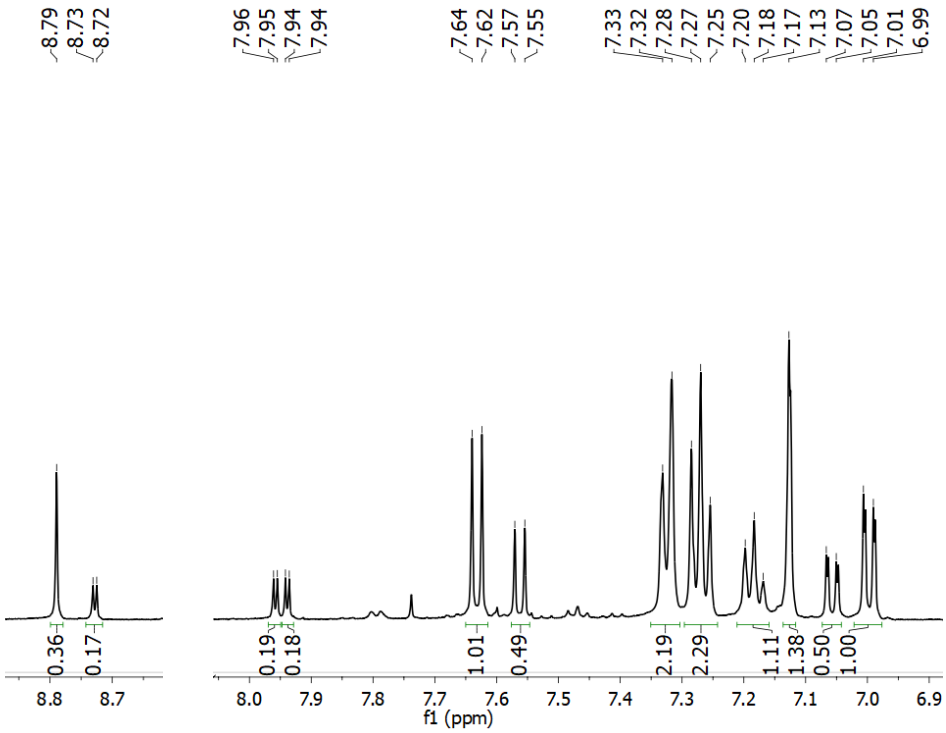

Figure S32. ^{1}H-NMR spectrum (aromatic region) of **pZr-1** after DNP sorption and overnight MeOH treatment, digested in D_2O/NaOD. Peaks corresponding to TNP and DNP found at δ (ppm) 8.79 and δ (ppm) 8.72, 7.96, 7.94, respectively.

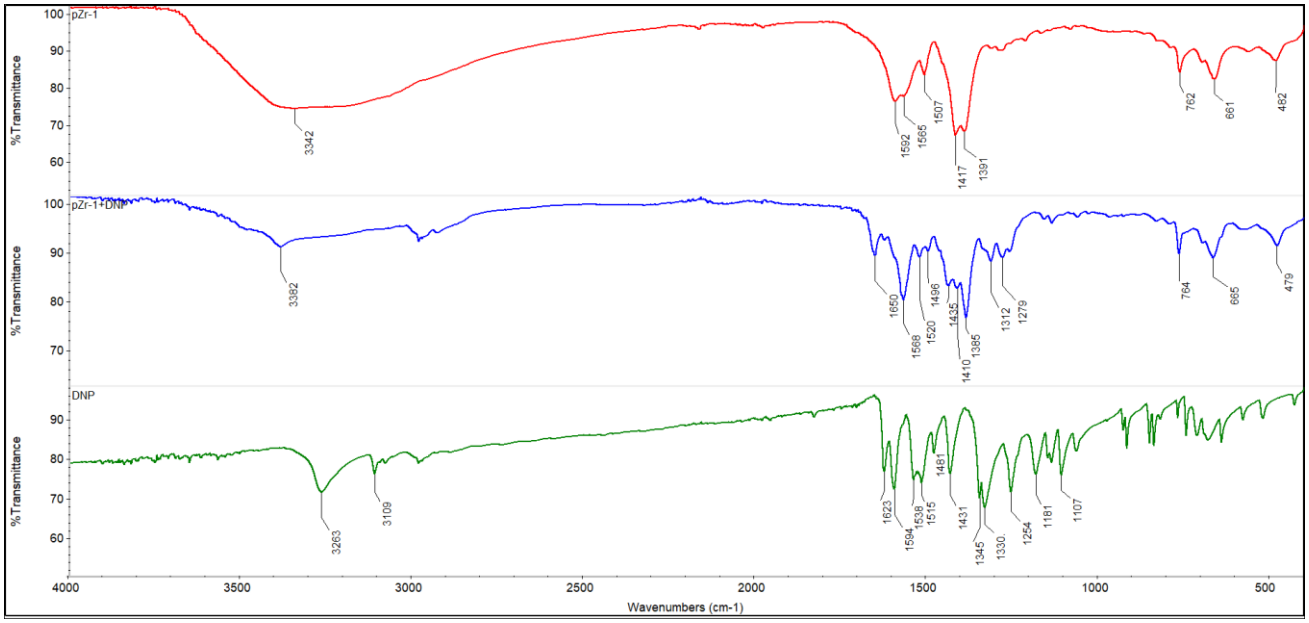

Figure S33. IR spectra of **pZr-1** (red line), **pZr-1** after DNP sorption (blue line) and DNP (green line).

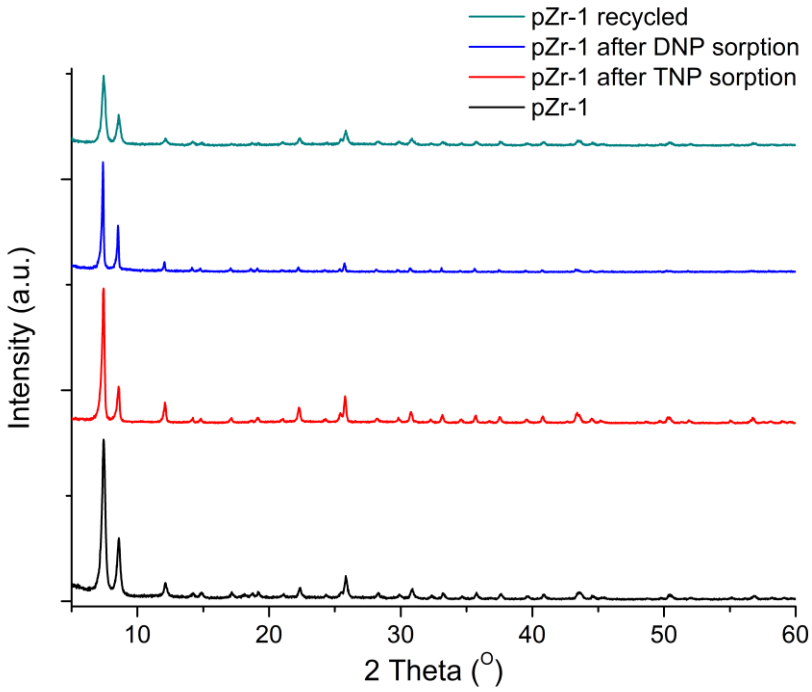

Figure S34. PXRD patterns of **pZr-1** (black line), **pZr-1** after TNP sorption (red line), **pZr-1** after DNP sorption (blue line) and **pZr-1** after TNP sorption acid re-activation (green line).

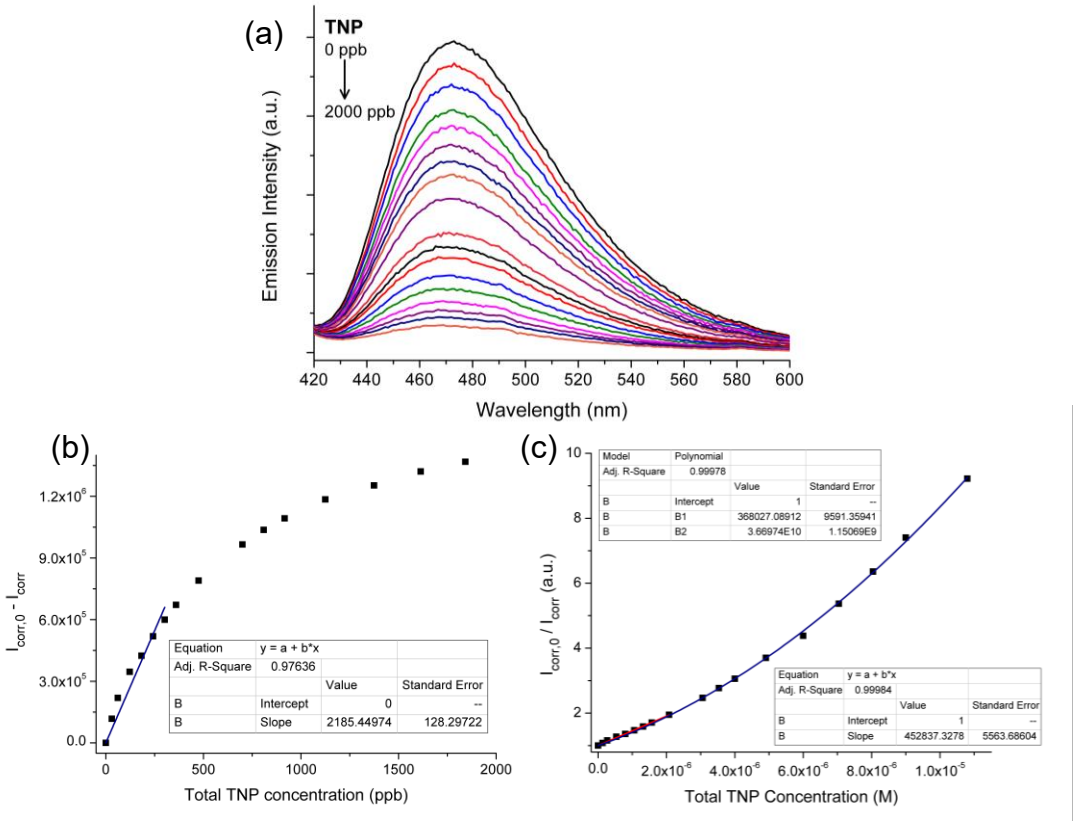

Figure S35. (a) Fluorescence titration (λ_{exc} = 400 nm) of recycled **pZr-1** suspended in H_2O (2 mL, 0.1 mg mL^{-1}) at pH 4.5 upon gradual addition of aqueous solution of TNP (5×10^{-5} M) with the corresponding (b) calibration curve and (c) Stern-Volmer plot.

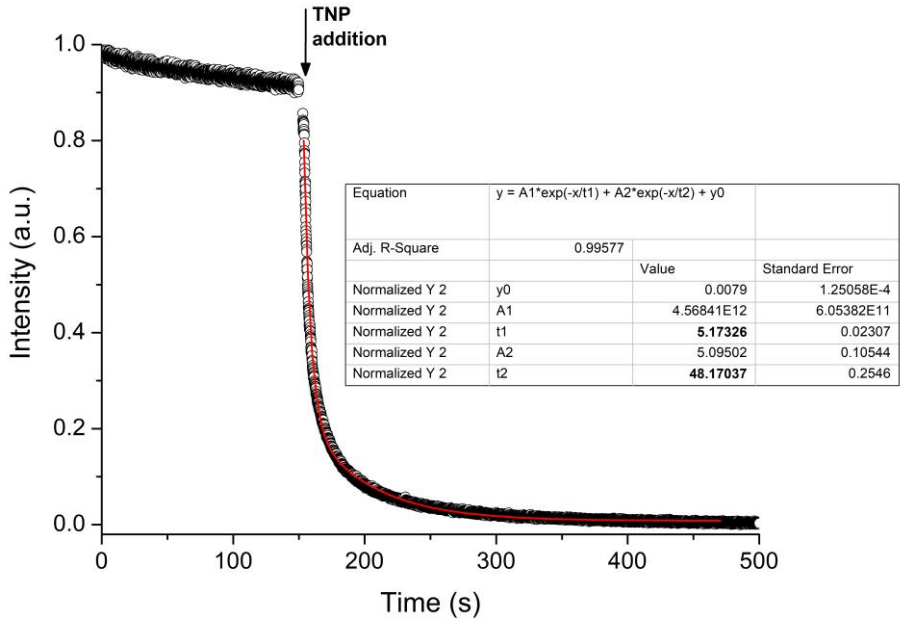

Figure S36. Time-dependent fluorescence response (λ_{exc} = 400 nm, λ_{em} = 470 nm) of **pZr-1** suspended in H_2O (2 mL, 0.1 mg mL^{-1}) at pH 4.5 upon addition of 25 µL of an aqueous solution of TNP (10^{-3} M). The concentration of TNP corresponds to that at the end of a typical titration experiment (8 µM). Black circles represent experimental data, the red curve represents the best fit based on a double exponential decay.

Table S1. Representative examples of luminescent MOF sensors for TNP and DNP.

Luminescent MOF	Analyte	Solvent	LOD (μM)	K_{SV} (M^{-1})	λ_{exc} (nm)	$\lambda_{em,max}$ (nm)	Ref.
$[Cd^3(L)_3(oba)_3]_n$	TNP	DMF	2.5	-	-	430	[6]
$\{[(CH_3)_2NH_2]_2[Cd_3(L)_2(BDC)]\cdot 4DMF\}_n$	TNP	DMF	-	9.65×10^4	311	440	[7]
$[Zn_2(TCPE)(tta)_2]\cdot 2DMF\cdot 4H_2O\cdot 2Me_2NH_2^+$	TNP	DMF	0.036	3.06×10^4	392	461	[8]
	DNP		0.029	3.75×10^4			
$\{(Me_2NH_2)_{10}[Zn_6L_4(\mu_3O)2Zn_3]\cdot G_x\}_n$	DNP	DMF	2.86	5.11×10^4	340	435	[9]
Amine-CQDs@UiO-67	DNP	DMF	0.005	1.4×10^3	365	440	[10]
$\{[Zn(L)]\cdot 2MeOH\cdot H_2O\}_n$	TNP	DMF	0.11	3.21×10^4	350	536	[11]
$Zr_6O_4(OH)_4(L)_6$	TNP	H_2O	2.6	2.9×10^4	320	438	[12]
$[Eu_3(bpydb)_3(HCOO)(\mu_3\text{-}OH)_2(H_2O)]$	TNP	H_2O	4.98	2.1×10^4	362	615	[13]
$[Zn_8(ad)_4(BPDC)_6O\cdot 2Me_2NH_2]\cdot G$	TNP	H_2O	0.012	4.6×10^4	340	405	[14]
$[Zn_4(DMF)(Ur)_2(NDC)_4]$	TNP	H_2O	7.1	10^5	310	400	[15]
$Zr_6O_4(OH)_4(L)_6$	TNP	H_2O	1.75	5.8×10^4	395	500	[16]
$[Cd(NDC)L]_2\cdot H_2O$	TNP	H_2O	-	3.7×10^4	370	400	[17]
$[Cd(5\text{-}BrIP)(TIB)]_n$	TNP	H_2O	0.27	2.7×10^4	300	431	[18]
$Zr_6O_4(OH)_8(H_2O)_4(CTTA)_{8/3}$	TNP	H_2O	0.1	3.1×10^5	312	381	[19]
$Zr_6O_4(OH)_8(H_2O)_4(TTNA)_{8/3}$	TNP	H_2O	0.043	5.1×10^5	324	399	
$\{[Tb_2(L)_3(H_2O)_2]\cdot 21H_2O\}_n$	TNP	H_2O	0.29	1.5×10^4	260	548	[20]
$\{[Zr_6O_4(OH)_4(L)_6]\cdot 8H_2O\cdot 6DMF\}_n$	TNP	MeOH	1.63	2.49×10^4	370	510	[21]
UiO-68-mtpdc/etpdc	TNP	MeOH	-	2.8×10^4	370	490	[22]
	DNP		-	2.3×10^4			
$\{[Cd_2(L)_2(btc)Cl]\cdot G_x\}_n$	TNP	MeCN	-	1.6×10^5	278	386	[23]
$Zr_6(m_3\text{-}O)_4(m_3\text{-}OH)_4(OH)_6(TCA)_2(H_2O)_6)$	TNP	EtOH	0.362	2.6×10^5	365	454	[24]
$\{Zr_6O_{16}H_{16}$(**L-1**$)_{3.6}(NH_2\text{-}bdc)_{0.4}\}$	TNP	H_2O	0.011	7.2×10^5	400	470	**This work**
	DNP	H_2O	0.026	2.9×10^5			

References

[1] S. Rapti, D. Sarma, S. A. Diamantis, E. Skliri, G. S. Armatas, A. C. Tsipis, Y. S. Hassan, M. Alkordi, C. D. Malliakas, M. G. Kanatzidis, T. Lazarides, J. C. Plakatouras, M. J. Manos, *J. Mater. Chem.*, 2017, **5**, 14707-14719.

[2] A. Schaate, P. Roy, A. Godt, J. Lippke, F. Waltz, M. Wiebcke, P. Behrens, *Chem. Eur. J.*, 2011, **17**, 6643-6651.

[3] L. Valenzano, B. Civalleri, S. Chavan, S. Bordiga, M. H. Nilsen, S. Jakobsen, K. P. Lillerud, C. Lamberti, *Chem. Mater.*, 2011, **23**, 1700-1718.

[4] a) S. Chen, Y.-L. Yu, J.-H. Wang, *Anal. Chim. Acta*, 2018, **999**, 13-26; b) M. Kubista, R. Sjöback, S. Eriksson, B. Albinsson, *Analyst* 1994, **119**, 417-419.

[5] D. MacDougall, W. B. Crummett, *Anal. Chem.*, 1980, **52**, 2242-2249.

[6] Z.-J. Wang, L. Qin, J.-X. Chen, H.-G. Zheng, *Inorg. Chem.*, 2016, **55**, 10999-11005.

[7] Q. Wang, D. J. Liu, L. L. Cui, X.-L. Hu, X.-L. Wang, Z.-M. Su, *New J. Chem.*, 2019, **43**, 963-969.

[8] X. Zhang, G. Ren, M. Li, W. Yang, Q. Pan, *Cryst. Growth Des.*, 2019, **19**, 6308-6314.

[9] Y. Zhang, S. Yuan, G. Day, X. Wang, X. Yang, H.-C. Zhou, *Coord. Chem. Rev.*, 2018, **354**, 28-45.

[10] Z. Wei, R.-N. Yang, J.-M. Yang, S.-S. Ji, X. Jiang, S.-Z. Mi, X.-L. Song, Y.-Y. Wang, Q. Wang, *Russ. J. Phys. Chem. A*, 2019, **93**, 2452-2457.

[11] Q. Sun, K. Yang, W. Ma, L. Zhang, G. Yuan, *Inorg. Chem. Front.*, 2020, **7**, 4387-4395.

[12] S. S. Nagarkar, A. V. Desai, S. K. Ghosh, *ChemComm*, 2014, **50**, 8915-8918.

[13] X.-Z. Song, S.-Y. Song, S.-N. Zhao, Z.-M. Hao, M. Zhu, X. Meng, L.-L. Wu, H.-J. Zhang, *Adv. Funct. Mater.*, 2014, **24**, 4034-4041.

[14] B. Joarder, A. V. Desai, P. Samanta, S. Mukherjee, S. K. Ghosh, *Chem. Eur. J.*, 2015, **21**, 965-969.

[15] S. Shanmugaraju, P. S. Mukherjee, *Chem. Eur. J.*, 2015, **21**, 6656-6666.

[16] S. S. Nagarkar, A. V. Desai, P. Samanta, S. K. Ghosh, *Dalton Trans.*, 2015, **44**, 15175-15180.

[17] B.-Q. Song, C. Qin, Y.-T. Zhang, X.-S. Wu, L. Yang, K.-Z. Shao, Z.-M. Su, *Dalton Trans.*, 2015, **44**, 18386-18394.

[18] Y. Rachuri, B. Parmar, K. K. Bisht, E. Suresh, *Dalton Trans.*, 2016, **45**, 7881-7892.

[19] B. Wang, X.-L. Lv, D. Feng, L.-H. Xie, J. Zhang, M. Li, Y. Xie, J.-R. Li, H.-C. Zhou, *J. Am. Chem. Soc.*, 2016, **138**, 6204-6216.

[20] R. Fu, S. Hu, X. Wu, *J. Mater. Chem. A*, 2017, **5**, 1952-1956.

[21] M. Sk, S. Biswas, *CrystEngComm*, 2016, **18**, 3104-3113.

[22] Q.-Y. Li, Z. Ma, W.-Q. Zhang, J.-L. Xu, W. Wei, H. Lu, X. Zhao, X.-J. Wang, *ChemComm*, 2016, **52**, 11284-11287.

[23] X.-S. Zeng, H.-L. Xu, Y.-C. Xu, X.-Q. Li, Z.-Y. Nie, S.-Z. Gao, D.-R. Xiao, *Inorg. Chem. Front.*, 2018, **5**, 1622-1632.

[24] H. Xu, F. Zhong, F. Chen, T.-X. Luan, P. Li, S. Xu, J. Gao, *J. Mater. Chem. C*, 2022, **10**, 7469-7475